Taylor & Francis
Taylor & Francis Group

Automatika

Journal for Control, Measurement, Electronics, Computing and Communications

ISSN: (Print) (Online) Journal homepage: https://www.tandfonline.com/loi/taut20

Angular symmetrical components-based anti-islanding method for solar photovoltaic-integrated microgrid

V. Arivumani & Sujatha Balaraman

To cite this article: V. Arivumani & Sujatha Balaraman (2023) Angular symmetrical components-based anti-islanding method for solar photovoltaic-integrated microgrid, Automatika, 64:1, 1-21, DOI: 10.1080/00051144.2022.2095829

To link to this article: https://doi.org/10.1080/00051144.2022.2095829

Published online: 05 Jul 2022.

AUTOMATIKA
2023, VOL. 64, NO. 1, 1–21
https://doi.org/10.1080/00051144.2022.2095829

REGULAR PAPER

OPEN ACCESS Check for updates

Angular symmetrical components-based anti-islanding method for solar photovoltaic-integrated microgrid

V. Arivumani[a] and Sujatha Balaraman[b]

[a]Department of Electrical and Electronics Engineering, Government College of Engineering, Bargur, Krishnagiri, India; [b]Department of Electrical and Electronics Engineering, Government College of Technology, Coimbatore, India

ABSTRACT

This article examines how an innovative Angular Symmetrical Components of Voltages be applied to islanding detection and voltage unbalance factor estimation at a photovoltaic inverter-based distribution unit. Positive and Negative Sequence Components are converted into a polar form such as Line Aggregate RMS (LARMS) Voltage and Tangent Angle of Unbalance (TAU) which are determined from two line voltage signals. Three voltage relays are replaced with a single relay which compares the LARMS voltage and TAU with threshold limits to identify the condition of balance. ASCOV relay does not generate the trip signal in a non-islanding situation such as linear load switching and nonlinear load switching. The Non-Detection Zone (NDZ) of this ASCOV relay is very low compared to other relays. The proposed anti-islanding method is tested in a SPV powered microgrid using MATLAB/SIMULINK and the performance was studied under islanding and non-islanding events. Consequently, the simulation outcome indicates that the proposed technique effectively identifies the islanding condition with less computation time as 1 s and the performance of the proposed relay is compared with existing relays. The voltage unbalance factor determined by the proposed method is very close to the actual value in all types of unbalance conditions.

ARTICLE HISTORY
Received 1 July 2021
Accepted 26 June 2022

KEYWORDS
Angular symmetrical components; generalized phase voltage; line aggregate RMS; tangent angle of unbalance; phase sequence index; non-detection zone; passive anti-islanding

1. Introduction

In power systems, renewable energy-dependent DGs are utilized for cost-effective and superior environmental performance. These generations use wind energy, solar energy and fuel cells [1]. The DGs must be equipped with superior Anti-Islanding Methods (AIM) as per IEEE Std 929-2000 [2] and IEEE Std 1547-2003 [3] for guarding the utility and DG and against switching, transients and dangers [4]. For isolation, the anti-islanding approaches sense the power system's abnormal condition and provide the trip signal to the circuit breaker for disconnecting the microgrid as a utility grid. After the disconnection of the power grid, the microgrid sends the local loads. The islanding recognition approaches are performed by comparing the parameters, such as power factor, voltage, frequency and so on, with a definite threshold value [5]. The microgrid consists of a three-phase inverter, PV model and three-phase parallel RLC Load. This microgrid is associated through the breaker to the grid for evaluating the anti-islanding techniques.

The anti-islanding techniques are mostly classified as Remote Anti-Islanding methods (RAIM) and Local Anti-Islanding methods (LAIM). LAIM may be categorized into active, passive and hybrid anti-islanding approaches [6]. For performing the operations, the remote anti-islanding techniques utilize the communication lines. It needs large costs for implementation [7]. Moreover, the passive anti-Islanding Methods (PAIM) are simply implemented with different measurement approaches. It creates more sensitivity, quick recognition and greater accuracy; however, it lacks implementation because of the large non-detection region and needless trips owing to greater sensitivity. For anti-islanding, the Overvoltage/Undervoltage and Over frequency/Under frequency is the simplest method [8]. However, it fails for detecting the condition in minor power mismatches. Several passive islanding recognition techniques are developed via sensing charge of parameter variation such as Rate of change of Active and Reactive Power [9], Rate of change of Frequency [10] and Voltage Phase Jump Detection [11]. Current passive islanding detection approaches are performed by recognizing the power system's unbalance condition. Voltage Unbalance (VU) and current THD are the latest technique among them [12].

Besides, the AIM are performed depending on the comparison of the frequency with the setting of the threshold value. These approaches execute their operation via Active Frequency Drift [13], Sandia Frequency Drift [14], Sandia Voltage Shift [15], Slip mode frequency shift [16], Reactive Power variation

CONTACT V. Arivumani arivu2021@aol.com, sujaengg@gmail.com

[17] and Voltage Positive Feedback [18]. The NDZ in this approach is little contrasted to the passive anti-islanding techniques. Nevertheless, it reduces the quality of the power because of the variation in the supply via initiating the disturbances. Besides, the Hybrid Anti-Islanding method (HAIM) combines the operation of Passive Anti-islanding and Active Anti-Islanding methods. Voltage Unbalance/Total Harmonic Distortion and Positive Feedback [19], and Average Rate of Change of Voltage and Real Power Shift [20] are the finest hybrid islanding detection approaches. However, the implementation is very multifaceted and recognition time is hugely contrasted to other techniques.

Several investigation works have earlier existed at bibliography that relied on the anti-islanding technique for photovoltaic inverter-based distributed generation systems. Some of them are reviews that were followed.

S. Manikonda et al. [21] have developed a novel islanding detection approach depending on image classification with a support vector machine (SVM). The oriented gradient characteristics histogram was removed from the image of classifying islanding and non-islanding events. Here, the time-series signal obtained from PCC was changed into an image. For testing and training multiple SVM classifiers, the oriented gradient characteristics histogram was removed as an image that was utilized as an input feature vector. The rate of change of voltage and rate of change of negative sequence voltages were utilized. Besides, early islanding detection was introduced for recognizing an islanding condition even earlier than it has happened. B. Cuka et al. [22] have presented the innovative islanding detection approach for single-phase inverter-based distributed generation. Primarily, autoregressive signal modelling was used for extracting the features of the signal from current and voltage signals at the PCC with the grid. After that, an advanced machine learning system depends on the support vector machine that receives the calibrated characteristics as inputs were used for forecasting the islanding condition. This study is implemented on IEEE 13 bus system for various islanding and non-islanding states. J. Reddy et al. [23] have developed the hybrid system for islanding recognition of DG. The control design presented was a hybrid implementation of Random Forest (RF) and Moth Flame Optimization (MFO), hence it was named RFMFO. The purposes of the presented work were to decrease the NDZ as near to possible and keep the quality of the power output unaltered. The rate of change of frequency (ROCOF) was utilized at the DG target location and utilized as input sets for an RF system. For intelligent islanding detection, RF precision was prepared through the MFO algorithm. Besides, RF is used to recognize islanding and non-islanding conditions. Some conditions and various load, switching operation and network conditions were resolved to approve the practicality of the presented approach.

N. Bhatt et al. [24] have introduced the passive islanding detection approach that depends on modal current and adaptive impulse. The three-phase currents of the target distributed generation system were changed into modal signals that decrease the data set. Such modal currents were decomposed in mono-frequency components using the empirical mode decomposition tool. Furthermore, the authentic mono-frequency components are recognized via correlation, which was changed by the Hilbert transform. The signal/noise ratio, skewness, kurtosis, entropy, power and total harmonic distortion were attained from the Hilbert transform. Consequently, such characteristics function as input for the adaptive drive approach to classify islanding and non-islanding states.

S. Vyas et al. [25] have developed computational intelligence-dependent approaches to address islanding problems on power grids that have associated renewable energy-dependent DGs. The different approaches reported have been evaluated based on their working technologies, accuracy, instruments utilized, speed and other relevant features. In light of the current state of the art required to include more resilience to the operation of distributed generation systems connected to the grid, an innovative perspective was talked about, with beginning outcomes, for addressing the problem of islanding, which may be used as an efficient approach through public services to guarantee a smoother operation of the power grid.

J. Jo et al. [26] have presented the reactive power variation approach that depends on positive feedback for enhancing islanding detection in DGs. Initially inserting a constant reactive power and then inserting a reactive power that improves infinitely with positive feedback. The initial part provides the activation of positive feedback by changing the frequency of PCC to some operating point under the islanding state. Then, the second division performs a significant role in accelerating the frequency shift towards the upper/lower threshold level. Because of the amalgamation of the two parts, this approach does not have a non-detection region, and it has better performance despite the load conditions.

For a parallel multi-PV system, J. Ke et al. [27] have introduced the passive intelligent IDM based on the enhanced Adaptive Boosting (Adaboost) algorithm. The presented approach generates the classification models for recognizing the islanding to avoid the passive approaches NDZ. For adjusting the classification model and enhancing the recognition capability, these approaches take the advantage of the electrical correlation between feature parameters through redistributing each sub-model weight. The simulation outcome demonstrates that these approaches can efficiently differentiate the islanding operation in the conventional passive IDMs NDZs.

A review of current investigation work indicates that the identification of islanding problems is an important contributing factor to DGs. The islanding condition mainly occurs due to the line fault and can cause a definite hazard on microgrids with distributed energy. These islanding faults critically concern the common DGs activity. Several research works presented numerous techniques for solving the islanding issues. They are communication-based active, passive and hybrid approaches. The communication-dependent approaches are more expensive than the dissimilar methods due to the necessity for establishing the guarantee system and reconfiguring the defence method. Furthermore, islanding mode following and varying exact parameters of the network, such as reactive power, voltage and frequency, are supposed through localized algorithms, such as passive and active approaches. However, the passive approaches to detect the islanding condition are neglected while the system has a small power imbalance. Besides, active methods are beneficial compared to passive approaches; however, threshold values are typically set experimentally which can be tricky and confusing. These aforementioned drawbacks are motivated by the existing systems that do this research work.

Therefore, for improving the performance of microgrids, a novel technique is selected for reducing these issues. In this paper, the ASCOV relay is proposed for a photovoltaic inverter-based distributed generation unit using new Angular symmetrical components (ASC). The main purpose of this manuscript is to recognize the islanding condition for avoiding the nuisance tripping of a circuit breaker during non-islanding events.

The contribution of the research is:

(1) Develop a method that examines how an innovative Angular Symmetrical Components of voltages be applied to islanding detection and voltage unbalance factor the estimation at photovoltaic inverter-based distribution unit.
(2) Propose a new strategy magnitude and angle relay combined as ASCOV relay that identifies the islanding condition.
(3) A non-detection zone (NDZ) of this ASCOV relay is very low compared to other relays.
(4) Consequently, the outcome indicates that the proposed methodology identifies the islanding condition with better recall and precision, less computation and reduces the complexity of the algorithm with an accuracy of 99%.

The rest of the manuscript is mentioned as below: Section 2 explains system modelling and design analysis. Section 3 describes the proposed technique and its process; in Section 4, simulations and results are obtained using objective functions of the proposed technique. Finally, the conclusion is presented in Section 5.

2. Modelling of solar photovoltaic-integrated microgrid

The islanding is considered a dangerous safety issue on a grid-connected photovoltaic system. In DG, the grid and photovoltaic systems are separated at the islanding situation. Grid parameters such as voltage and frequency are not stable during the islanding condition [28]. Through islanding mode, the fault is cleared through these conditions varying from the grid reference values through the circuit breaker (CB) connected between the common point (PCC) and the grid. DG still provides power to the local load if CB cannot clear the circuit. Due to the unusual interference of the grid, the islanding activity is caused in a photovoltaic system; these bizarre conditions occurred subject to equipment disappointment, voltage shutdown and short circuit conditions. The islanding in a PV depends on the DG system and includes a DC-DC step-up converter, solar PV array and a photovoltaic inverter together with their filter, which is illustrated in Figure 1. The mathematical model of these three main areas is explained in the following subsections.

2.1. Mathematical formulation of PV system

The solar cell is the fundamental element of the PV generation system. The photovoltaic cells are joined in series or in parallel to create the solar arrays with the necessary ratings. Figure 2 displays the equivalent circuit of the photovoltaic system [29]. In a photovoltaic energy subsystem, photovoltaic panels are utilized to change accumulated sunlight into electrical energy. The power generated through a photovoltaic system is calculated using the Equation (1)

$$P_{pv} = R_t \eta_{pv} A_{pv} \tag{1}$$

where P_{pv} denotes PV panels output power, R_t denotes solar radiation in the tilted plane module, η_{pv} indicates PV panels efficiency and A_{pv} is PV panel area. The below equation articulate the photovoltaic panel efficiency,

$$\eta_{pv} = \eta_{r-pv} \eta_{PC} [1 - N_T (T_C - T_{ref})] \tag{2}$$

where photovoltaic panel efficiency denotes η_{pv}, reference module efficiency indicates η_{r-pv}, power condition efficiency denotes η_{PC}, photovoltaic panel efficiency temperature coefficient is N_T, cell temperature (°C) is T_C and cell temperature in reference conditions is T_{ref}. If ideal maximal power tracker is utilized, η_{PC} value is equivalent to unity. Similarly, T_{ref} is placed at 25°C and also the temperature of mono- and polycrystalline silicon N_T as -3.7×10^{-3}°C^{-1}. Furthermore,

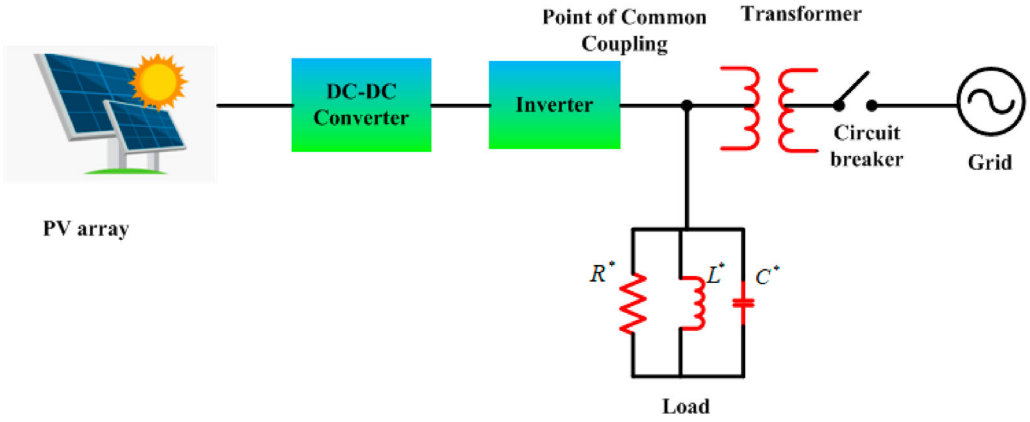

Figure 1. Schematic diagram of islanding mode in a grid-connected PV system.

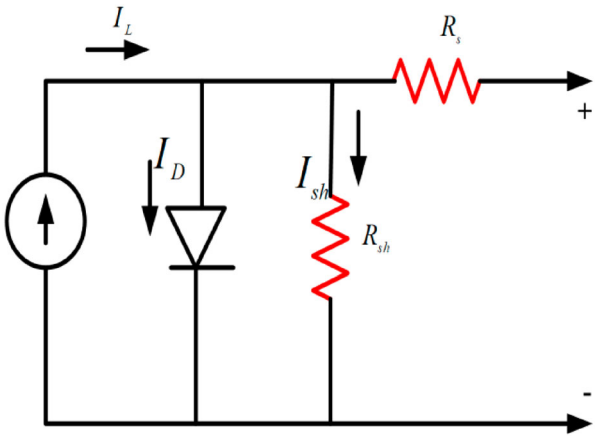

Figure 2. Modelling of the PV system.

T_C articulated as taken following,

$$T_C = T_A + \left(\frac{T_N - 20}{800}\right) R_t \tag{3}$$

Here, T_A denotes ambient air temperature, and T_N indicates nominal cell operating temperature. The PV module voltage–current relationship is expressed in Equation (4) as follows:

$$I = I_L - I_{sat}\left[\exp\left\{q\frac{V_{pv} + I_{pv}.R_s}{\upsilon k T_c}\right\} - 1\right] - \frac{V_{pv} + I_{pv}.R_s}{R_{sh}} \tag{4}$$

where I_L is the generated current of the Light in A, R_s and R_{sh} are the shunt and series resistances in Ω, υ is the ideality factor of p-n, k is the Boltzmann's constant, I_{pv} and V_{pv} are the solar cell output current and voltage, respectively, and I_{sat} is the reverse saturation current in A. The light-generated current I_L^* and reverse saturation current $I_{sat}*$ are illustrated in Equations (5) and (6), respectively.

$$I_L^* = [I_{sc} + \gamma(T_c - T_c^*)]\frac{C_T}{C_T^*} \tag{5}$$

$$I_{sat}^* = \frac{I_{sc}\gamma(T_c - T_c^*)}{\exp\left[\frac{V_{oc}\gamma(T_c - T_c^*)}{V_T}\right] - 1} \tag{6}$$

where T_c is the ambient temperature of the PV cell, C_T is the irradiance, γ is the temperature coefficient of the short circuit current, V_{oc} is the open-circuit voltage at standard temperature and V_T is the thermal voltage.

2.2. DC–DC converter model

For obtaining the ideal DC bus voltage, the DC–DC converter is significant. The passive elements, an inductor L and capacitor C of the converter are evaluated based on the following equation.

$$L = \frac{V_i(V_o - V_i)}{\Delta I_i f_s V_o} \tag{7}$$

$$C = \frac{I_0 D}{\Delta v f_s} \tag{8}$$

where D is the duty cycle which is estimated using Equation (9).

$$D = 1 - \left(\frac{V_i}{V_o}\right) \tag{9}$$

In the previous equation, the input current is taken as ΔI_i and boost converter outcome voltage is taken as Δv.

2.3. PV inverter model

DC voltage is converted into AC voltage through a three-phase voltage source converter (VSC). The PV inverter contains the six MOSFETs. At the stationary revolving frame, the voltage equation of the equivalent photovoltaic inverter model is represented in Equation (10).

$$V_c = R_f I_s + L_f \frac{d(I_s)}{dt} + V_s \tag{10}$$

3. Proposed anti-islanding ASCOV relay for photovoltaic inverter-based distributed generation

3.1. Generalized phase voltages and angular symmetrical components

For analysing the unsymmetrical faults happened in power system, the symmetrical component theory was utilized. Reference currents in Power electronic controllers are produced using this theory. The symmetrical components are utilized by transforming the unsymmetrical phasor values into sum of the symmetrical components series. They are categorized into the sequence of the zero, positive and negative (ZPN). This theory was comprehensive to time domain as instantaneous symmetrical components for estimating the conditions of the imbalance in the state of transient [30]. The instantaneous symmetrical components of voltages are changed from the actual phase voltages using Equation (11).

$$\begin{vmatrix} V_0(t) \\ V_p(t) \\ V_n(t) \end{vmatrix} = \frac{1}{\sqrt{3}} \begin{vmatrix} 1 & 1 & 1 \\ 1 & \alpha & \alpha^2 \\ 1 & \alpha^2 & \alpha \end{vmatrix} \begin{vmatrix} V_a(t) \\ V_b(t) \\ V_c(t) \end{vmatrix} \tag{11}$$

where V_0, V_p and V_n are the voltage of the zero, positive and negative sequence components, and α is the factor which representing 120° phase shift and α^2 is the complex conjugate of α which is given by,

$$\alpha = 1\angle 120^\circ = e^{j\frac{2\Pi}{3}} = -\frac{1}{2} + j\frac{\sqrt{3}}{2} \tag{12}$$

$$\alpha^2 = 1\angle 240^\circ = e^{-j\frac{2\Pi}{3}} = -\frac{1}{2} - j\frac{\sqrt{3}}{2} \tag{13}$$

The symmetrical components are expressed in complex form by the way of applying Equations (12) and (13) in (11). Real part and Imaginary part of negative and positive sequence voltages are identical. The imaginary part is identical to the half-line voltage. Real part of the positive/negative sequence is rewritten with actual phase voltage and zero-sequence voltage.

$$V_0(t) = \frac{V_a(t) + V_b(t) + V_c(t)}{\sqrt{3}} \tag{14}$$

$$V_p(t) = \frac{2V_a(t) - V_b(t) - V_c(t)}{2\sqrt{3}} + j\frac{V_b(t) - V_c(t)}{2} \tag{15}$$

$$V_n(t) = \frac{2V_a(t) - V_b(t) - V_c(t)}{2\sqrt{3}} - j\frac{V_b(t) - V_c(t)}{2} \tag{16}$$

$$V_p(t) = \frac{\sqrt{3}}{2}\left(V_a(t) - \frac{V_0(t)}{\sqrt{3}}\right) + \frac{1}{2}jV_{bc}(t) \tag{17}$$

$$V_n(t) = \frac{\sqrt{3}}{2}\left(V_a(t) - \frac{V_0(t)}{\sqrt{3}}\right) - \frac{1}{2}jV_{bc}(t) \tag{18}$$

Phase voltages are generalized by removing the zero-sequence component ($V_0/\sqrt{3}$) to analyse the unbalance systems. These voltages are referred as 'Generalized Phase Voltages (GPV)'. Sum of all GPVs is equal to zero even in the unbalanced system whereas the sum of actual phase voltages results in zero sequence component. GPV simplifies the unbalance calculations and NDZ estimation. GPVs can be determined from line voltages for easier measurements and processes. Any two-line voltages are needed to obtain GPV as shown in Equation (19). Now the symmetrical components are written as the complex form of GPV and line voltage as shown in Equations (20) and (21).

$$\begin{aligned} V_{ag}(t) &= V_a(t) - \frac{V_0(t)}{\sqrt{3}} \\ &= \frac{1}{3}(2V_a(t) - V_b(t) - V_c(t)) \\ &= \frac{1}{3}(2V_{ab}(t) + V_{bc}(t)) \end{aligned} \tag{19}$$

$$V_p(t) = \frac{1}{2}\left(\sqrt{3}V_{ag}(t) + jV_{bc}(t)\right) \tag{20}$$

$$V_n(t) = \frac{1}{2}\left(\sqrt{3}V_{ag}(t) - jV_{bc}(t)\right) \tag{21}$$

Figure 3(a) illustrates the Phasor diagram of Generalized phase voltage, line voltage, negative sequence and positive sequence voltage. Figure 3(b) illustrates the polar form of symmetrical components which simplifies the calculation of sequence voltages and unbalanced factors. Positive and Negative Sequence Component are converted into Radial Component and Angular Component. Radial Component is the tangential component of sequence voltages. The magnitude of the radial component is equal to the overall RMS of Line voltages. This voltage is referred to as "Line Aggregate Root Mean Square Voltage" and abbreviated as LARMS voltage (V_λ). Total power delivered by unbalanced line voltages are equal to the power delivered by equivalent balanced line voltages with the value equal to this LARMS Voltage. This voltage magnitude is also estimated with phase voltages and zero sequence voltages. Magnitude of the zero sequence component is directly estimated with phase voltage magnitudes and line voltage magnitudes using Equation (26). Angular Component is equal to the arc tangent of the voltage unbalance factor which is the ratio between negative and positive sequence components. So this component is referred

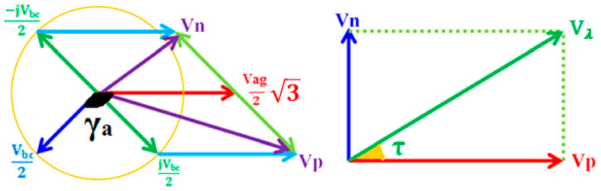

Figure 3. (a) Phasor diagram of generalized phase voltage, line voltage and symmetrical components. (b) Angular form of symmetrical components.

as "Tangent Angle of Unbalance (TAU)". This angle is used for performance analysis of unbalanced systems.

Let us consider the angle between GPV and Line voltage is represented by "γ_a". This angle is 90° in normal balanced condition. Radial and Angular components are determined from the phasor diagram.

$$\gamma_a = \angle V_{ag} - \angle V_{bc} \tag{22}$$

$$|V_p| = \frac{1}{2}\left(\sqrt{3V_{ag}^2 + V_{bc}^2 + 2\sqrt{3}V_{ag}V_{bc}\sin\gamma_a}\right) \tag{23}$$

$$|V_n| = \frac{1}{2}\left(\sqrt{3V_{ag}^2 + V_{bc}^2 - 2\sqrt{3}V_{ag}V_{bc}\sin\gamma_a}\right) \tag{24}$$

$$\begin{aligned} V_\lambda &= \sqrt{V_p^2 + V_n^2} = \frac{1}{\sqrt{2}}\sqrt{3V_{ag}^2 + V_{bc}^2} \\ &= \frac{1}{\sqrt{3}}\sqrt{V_{ab}^2 + V_{bc}^2 + V_{ca}^2} \\ &= \sqrt{V_a^2 + V_b^2 + V_c^2 - V_0^2} \end{aligned} \tag{25}$$

$$V_0 = \sqrt{(V_a^2 + V_b^2 + V_c^2) - \frac{1}{3}(V_{ab}^2 + V_{bc}^2 + V_{ca}^2)} \tag{26}$$

$$\begin{aligned} \tau &= \tan^{-1}\left(\frac{V_n}{V_p}\right) \\ &= \tan^{-1}\left(\sqrt{\frac{3V_{ag}^2 + V_{bc}^2 - 2\sqrt{3}V_{ag}V_{bc}\sin\gamma_a}{3V_{ag}^2 + V_{bc}^2 + 2\sqrt{3}V_{ag}V_{bc}\sin\gamma_a}}\right) \\ &= \tan^{-1}\left(\sqrt{\frac{1 - \sqrt{3}\frac{V_{ag}V_{bc}\sin\gamma_a}{V_\lambda^2}}{1 + \sqrt{3}\frac{V_{ag}V_{bc}\sin\gamma_a}{V_\lambda^2}}}\right) \end{aligned} \tag{27}$$

Actual voltage unbalance factor (μ) which is the ratio between negative sequence component and positive sequence component ranges from zero to infinity. In addition, based on the calculating method of unbalance factor, phase angle difference of positive and negative sequence component of three-phase voltage in the condition of supply voltage unbalance can be attained using Phase sequence indicator. Unbalanced voltages usually occur due to variation of loads. When the load of one or more within the phases is different from the other, unbalanced voltages will appear. This can be due to different impedances, or types and values of loading on each phase. Single phasing, which is the complete loss of a phase, is the ultimate voltage unbalance condition for a three-phase circuit.

The new factor is proposed for the islanding detection process that can determine the phase sequence of three-phase power system and is compatible with global utility grid frequencies. This identifies the status of unbalance. This value is positive if the positive sequence voltage is greater than the negative sequence. This value indicates the negative sign for phase reversal unbalance conditions. This factor is called as 'Phase Symmetrical Index (PSI – ψ)'. Relation between Phase Symmetrical Index and Voltage Unbalance Factor is illustrated in Figure 4(a). PSI is determined by the Generalized Phase voltage and Line voltage as explained in the following Equation (28). Table 1.

$$\begin{aligned} \psi &= \frac{V_p^2 - V_n^2}{V_p^2 + V_n^2} = \frac{1-\mu^2}{1+\mu^2} = \cos 2\tau \\ &= \sqrt{3}\frac{\mathrm{V_{ag}V_{bc}}\sin\gamma_a}{\mathrm{V_\lambda^2}} \end{aligned} \tag{28}$$

Elimination of GPV with line voltages is essential to simplify the calculation of PSI and TAU. Phase diagram has been drawn delineating the relation between GPV at phase "A" and Line voltages (V_{ab} and V_{bc}) as shown in Figure 4(b). Vertical component of $2V_{ab}$ and $3V_{ag}$ is equal and it is taken as V_y (Arbitrary Voltage). Phase angle between two-line voltages (V_{ab} and V_{bc}) is taken as δ_b. Magnitude and Phase angle of GPV are eliminated with the magnitude and phase angle of line voltage (V_{ab}) with the help of Equation (30). So the calculation needs only two-line voltages which reduces the burden of design. In LARMS Voltage calculations as shown below, third line voltage (V_{ca}) is eliminated and also phase angle is incorporated using the other two-line voltages (V_{ab} and V_{bc}). PSI, TAU and Voltage unbalance factors are expressed with two-line voltage magnitudes and the phase angle between line voltages.

$$\delta_b = \angle V_{ab} - \angle V_{bc} \tag{29}$$

$$V_y = 2V_{ab}\sin\delta_b = 3V_{ag}\sin\gamma_a \tag{30}$$

$$V_{ca}^2 = V_{ab}^2 + V_{bc}^2 + 2V_{ab}V_{bc}\cos\delta_b \tag{31}$$

$$\begin{aligned} V_\lambda^2 &= \frac{V_{ab}^2 + V_{bc}^2 + V_{ca}^2}{3} \\ &= \frac{2}{3}(V_{ab}^2 + V_{bc}^2 + V_{ab}V_{bc}\cos\delta_b) \end{aligned} \tag{32}$$

$$\psi = \sqrt{3}\frac{V_{ab}V_{bc}\sin\delta_b}{V_{ab}^2 + V_{bc}^2 + V_{ab}V_{bc}\cos\delta_b} \tag{33}$$

$$\begin{aligned} \tau &= \frac{1}{2}\cos^{-1}\psi \\ &= \frac{1}{2}\cos^{-1}\left(\sqrt{3}\frac{V_{ab}V_{bc}\sin\delta_b}{V_{ab}^2 + V_{bc}^2 + V_{ab}V_{bc}\cos\delta_b}\right) \end{aligned} \tag{34}$$

$$\begin{aligned} \mu &= \tan\tau \\ &= \tan\left(\frac{1}{2}\cos^{-1}\left(\sqrt{3}\frac{V_{ab}V_{bc}\sin\delta_b}{V_{ab}^2 + V_{bc}^2 + V_{ab}V_{bc}\cos\delta_b}\right)\right) \end{aligned} \tag{35}$$

Voltage unbalance factors are varied as per definitions by National Electronics Manufacturers Association (NEMA), IEEE, Pillay's approximation method (PAM) [31] and CIGRE [32]. These definitions need the RMS values of three-line voltages. The true voltage unbalance factor is near to the CIGRE definition.

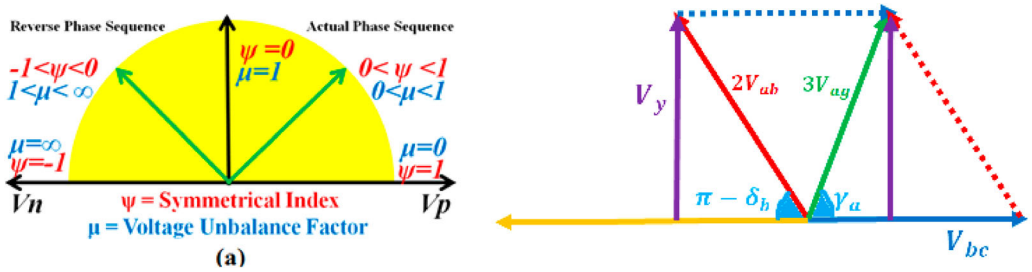

Figure 4. (a) Phase symmetrical index and voltage unbalance factor for normal and reverse phase sequences, (b) Relation between generalized phase voltage and line voltages.

Table 1. Voltage unbalance factor, tangent angle of unbalance and magnitude of unbalance for various unbalance conditions.

		Voltage unbalance factor (VUF)	Tangent angle of unbalance (TAU)	Phase sequence index (PSI)
SI No	Condition	μ	T	Ψ
1	Balanced Condition $V_n = 0$	0	0°	1
2	$V_n < V_p$	$0 < \mu < 1$	$0° < \tau < 45°$	$0 < \psi < 1$
3	$V_n = V_p$	$\mu = 1$	$\tau = 45°$	$\psi = 0$
4	Reverse Phase Sequence $V_n > V_p$	$1 < \mu < \infty$	$45° < \tau < 90°$	$-1 < \psi < 0$
5	Reverse Phase Sequence $Vp = 0$	$\mu = \infty$	$\tau = 90°$	$\psi = -1$

But this value is inaccurate for phase reversal conditions. The proposed method is 100% accurate because the PSI polarity is changed to negative if phase sequence is changed. Expressions to determine the voltage unbalance factors under various definitions are shown in Equations (36)–(40)

$$\mu_{NEMA} = \frac{\max(V_{ab} - V_{avg,line}, V_{bc} - V_{avg,line}, V_{ca} - V_{avg,line})}{V_{avg,line}} \times 100(\%) \quad (36)$$

$$\mu_{IEEE1} = \frac{\max(V_a - V_{avg,phase}, V_b - V_{avg,phase}, V_c - V_{avg,phase})}{V_{avg,phase}} \times 100(\%) \quad (37)$$

$$\mu_{IEEE2} = \frac{\max(V_a, V_b, V_c) - \min(V_a, V_b, V_c)}{V_{avg,phase}} \times 100(\%) \quad (38)$$

$$\mu_{PAM} = 82 \times \frac{\sqrt{(V_{ab} - V_{avg,line})^2 + (V_{bc} - V_{avg,line})^2 + (V_{ca} - V_{avg,line})^2}}{V_{avg,line}} (\%) \quad (39)$$

$$\mu_{CIGRE} = \frac{\sqrt{1 - \sqrt{3 - 6\beta}}}{\sqrt{1 + \sqrt{3 - 6\beta}}} \times 100(\%), \text{ where } \beta = \frac{V_{ab}^4 + V_{bc}^4 + V_{ca}^4}{(V_{ab}^2 + V_{bc}^2 + V_{ca}^2)^2} \quad (40)$$

3.2. Proposed anti-islanding method

The proposed ASCOV-ID (Angular Symmetrical Components Of Voltages-Islanding Detection) schematic block diagram is represented in Figure 5. The two-line voltages V_{ab} and V_{bc} are given as input. The RMS values of line voltages and phase angle difference can be evaluated through the Fourier Block. Furthermore, the Angular Symmetrical Components block is utilized for determining the LARMS Voltage (V_λ) and TAU (τ). The value of V_λ is compared to maximal and minimal threshold values and TAU is contrasted with utmost threshold angle (1°). In this paper, the rated voltage value is considered as 400 V. Therefore, the maximum and minimum voltage limits are 440 V (110%) and 352 V (88%). For providing the trip signal to circuit breaker, the logic signals produced from angle relay and magnitude relay are joined with the OR gate. Besides, the magnitudes of Voltage Unbalance factor and sequence components are estimated using τ and V_λ. The output trip signal is contrasted with over frequency/under frequency, voltage/under voltage Relay, THD relay and Voltage Unbalance. If the islanding is suspected, then the trip signal is sent for identifying the islanding. Operating Region of Voltage, Angle and combined relay is illustrated in Figure 6. Positive and Negative sequence components are placed in horizontal and vertical axis respectively.

The enhanced penetration of distributed generation based on inverter DG needs a sufficient plane of monitoring and recognition in islanding conditions. The islanding occurs while the DG system is disconnected from the rest of the power grid. Numerous approaches have been presented for detecting the islanding condition with low power mismatches. In this paper, angle-based islanding method is introduced in addition to voltage and frequency relays because angle variation is more sensitive than the voltage magnitude and frequency. The angle-based islanding technique is a passive islanding detection approach. Angle-based

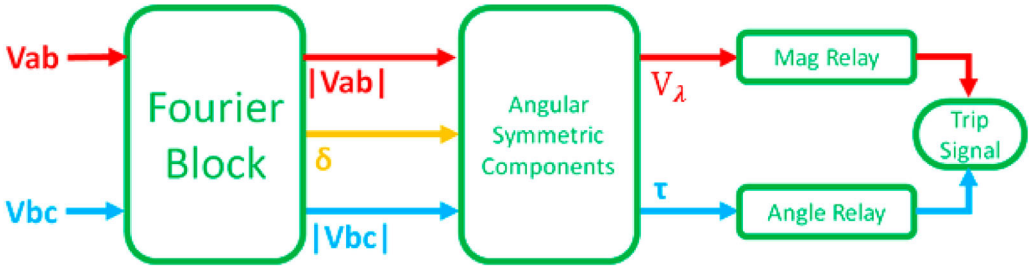

Figure 5. Proposed ASCOV islanding detection schematic block diagram.

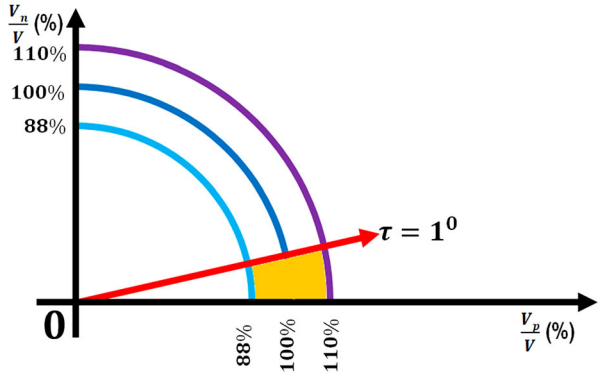

Figure 6. Operating region of voltage relay, angle relay and combined relay.

islanding technique is utilized for detecting the islanding mode depending on the calculated rate of change of frequency and voltage. This approach is triggered only when the rate of change of frequency and voltage phasor are higher than the certain threshold value for the frequency change rate and least voltage. If the threshold values are placed to be too small, it can consequence the needless trip of DG and if threshold values are set too large then the islanding cannot be identified. The relay would send a trip signal for activating the ASC components if the islanding is suspected. Then, ASC components will identify the islanding. Operating region of Voltage relay, Angle relay and ASCOV relay are shown in Figure 9.

3.2.1. Step by step process of angle-based islanding method for solar photovoltaic-integrated microgrid

Step 1: Initialization

The two-line voltages (V_{ab} and V_{bc}) are measured. All calculations required only two-line voltages instead of measuring three-phase voltages.

Step 2: RMS and phasor estimation

Fundamental components of line voltages are extrac ted via Fourier block. The RMS values of these line voltages and its phase angle are determined. The discrete Fourier transform is utilized to identify the generalized phase voltages and angular symmetrical components as these waveforms are in discrete time. The procedure employed for calculating the signal phase considers a range of N samples for each cycle. The first phasor angle is calculated when the N samples have been acquired while the second one begins at the sample $k = 1$ and ends at $k = N$.

Step 3: LARMS Voltage and Tangent Angle of Unbalance calculation

LARMS Voltage (V_λ) is determined with the RMS values of three-line voltages as shown in Equation (33). Tangent Angle of Unbalance is calculated using the RMS values of Line voltages and Phase Angle (δ_b) via Phase Sequence Index using Equation (35).

Step 4: Comparison with Thresholds

LARMS Voltage is identical to the rated line voltage in normal condition. So this magnitude is compared with Minimum and Maximum Voltage limits as shown in Equation (41).

$$88\% < \frac{V_\lambda}{V_{rated}} < 110\% \tag{41}$$

TAU value is oscillating near 0° in normal condition. The threshold limit of TAU is arbitrarily chosen as 1°. The angle is always positive which lies in the first quadrant. The operating limits of TAU values are mentioned in Equation (42).

$$\tau < 1^0 \tag{42}$$

Step 5: Verification of islanding condition

Voltage relay verifies the islanding condition of the system by comparing the LARMS voltage with threshold limits. An angle relay is added in addition to the voltage relay to improve the accuracy of the anti-islanding process. The relay is operated with the TAU parameter by comparing it with the threshold limit. The trip signal is generated if any of these relays are activated. So OR gate operation is required for this process.

If parameters lie in the limit, then go to step 2.

These procedures are illustrated in the flow chart as shown in Figure 7.

3.3. Non-detection zone of ASCOV relay

The NDZ is a valuable index to predict the possible missed operations of some relays in certain conditions. In addition to the type of relay and its settings, the NDZ also depends on the type of DG and its implemented control. Non-detection zone of voltage and frequency relay is very large. Anti-islanding process using this

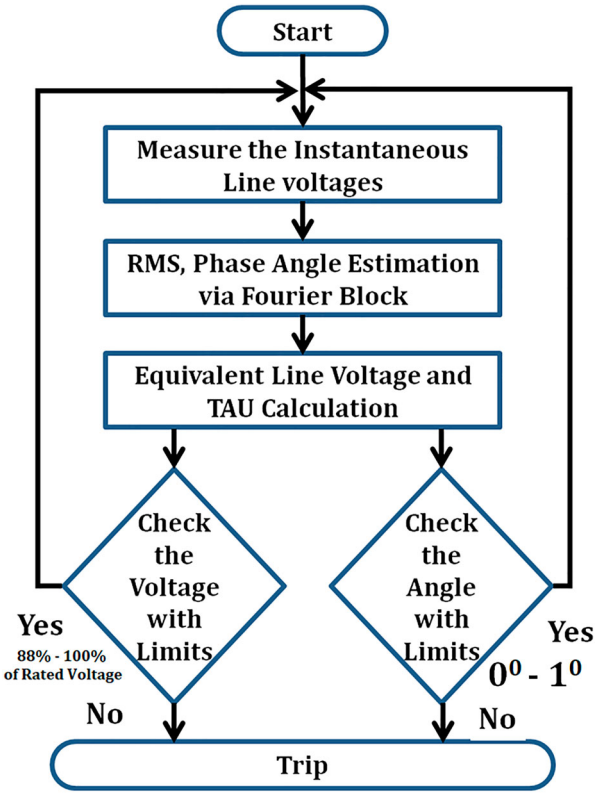

Figure 7. Flowchart of the ASCOV relay.

method affects the accuracy of the system. Angle-based relays will determine the islanding condition with very less time. It has low NDZ compared to other relays. The operation of this relay does not require any additional process. The voltage relay NDZ is expressed by the following equations.

$$\left(\frac{V_\lambda}{V_{max}}\right)^2 - 1 < \frac{\Delta P}{P} < \left(\frac{V_\lambda}{V_{min}}\right)^2 - 1 \tag{43}$$

$$-17.36\% < \frac{\Delta P}{P} < 29.13\% \tag{44}$$

Passive techniques require the critical setting of the threshold values as lower threshold settings may result in nuisance tripping, and higher values can lead to non-detection of islanding. The rate of change of frequency decreases when the active power mismatch decreases during islanding. Setting a threshold in the relay fails to detect islanding during some instances of active power mismatch during islanding. The mismatch of reactive power causes the frequency shift after islanding occurs. Therefore, a certain ratio of reactive power to active power is required to deviate the frequency out of a specified over/under the threshold.

NDZ of angle relay is evaluated through instantaneous reactive and active power via the ASC components. Non-detection zone is calibrated with mismatch limits of reactive and real power. Active and reactive power in a three-phase unbalanced system is expressed in terms of GPV and Line components. Generalized Current Component (I_{ag}) is introduced as the current component after the removal of zero sequence component. Equivalent Line Current (I_{bc}) is also introduced as the difference between two-phase currents.

$$I_{ag}(t) = I_a(t) - \frac{I_0(t)}{\sqrt{3}} \tag{45}$$

$$I_{bc}(t) = I_b(t) - I_c(t) \tag{46}$$

$$P = V_0 I_0 \cos \emptyset_0 + \frac{3}{2} V_{ag} I_{ag} \cos \emptyset_{ag} + \frac{1}{2} V_{bc} I_{bc} \cos \emptyset_{bc} \tag{47}$$

$$Q = \frac{\sqrt{3}}{2}(V_{bc} I_{ag} \cos \emptyset_1 - V_{ag} I_{bc} \cos \emptyset_2) \tag{48}$$

where Φ_0 = Angle between V_0 and I_0; Φ_{ag} = Angle between V_{ag} and I_{ag}; Φ_{bc} = Angle between V_{bc} and I_{bc}; Φ_1 = Angle between V_{bc} and I_{ag}; Φ_2 = Angle between V_{ag} and I_{bc}

Angles between GPV and line components of voltages and currents are illustrated in Figure 8. Reduced Phase Voltage (V_{ag}) is taken as reference. Phase angles represented in the reactive power formula are replaced with power angles (Φ_{ag} and Φ_{bc}) and Generalized Phase Angle (γ_a). Reactive power is affected by the Generalized Phase Angle. Reactive power is replaced with two equations

$$Q = \frac{\sqrt{3}}{2}(V_{bc} I_{ag} \cos(\gamma_a - \emptyset_{ag}) - V_{ag} I_{bc} \cos(\gamma_a + \emptyset_{bc})) \tag{49}$$

These power equations are simplified by following assumptions.

(1) Zero sequence components are neglected for small variations of voltages.
(2) Power factor angle of Generalized components is identical to Line components ($\Phi ar = \Phi bc = \Phi$).
(3) Ratio between Generalized current component and generalized voltage component is identical to the ratio between equivalent line current and line

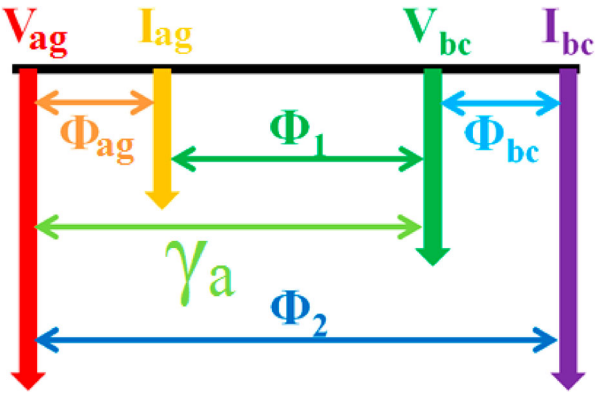

Figure 8. Angle between generalized phase components and line components of voltages and currents.

voltage.

$$\frac{I_{ag}}{V_{ag}} = \frac{I_{bc}}{V_{bc}} = \mathrm{G} \tag{50}$$

Now power equations are simplified with the above assumptions to identify the non-detection zone. The ratio between Reactive power and real power is equal to the product of the power factor angle (Φ) and PSI (ψ) is expressed as:

$$P = GV_{\lambda}^{2}\cos\emptyset \tag{51}$$

$$Q = \sqrt{3}GV_{ag}V_{bc}\sin\gamma_a \sin\emptyset \tag{52}$$

$$\frac{Q}{P} = \frac{\sqrt{3}V_{ag}V_{bc}\sin\gamma_a}{V_{\lambda}^{2}}\tan\emptyset = \psi\tan\emptyset \tag{53}$$

Let P_0 and Q_0 are the initial reactive powers under balanced conditions. The powers in unbalanced systems are written as the sum of initial power and incremental power. The reactive power to real power ratio is equal to the tangent of power factor angle. The proposed islanding method compares the TAU with threshold. The power factor angle is assumed to be constant in small variations.

$$\frac{Q_0 + \Delta Q}{P_0 + \Delta P} = \psi\tan\emptyset = \psi\frac{Q_0}{P_0} \tag{54}$$

$$\left(\frac{\Delta Q}{P_0}\right) = \psi\tan\emptyset\left(\frac{\Delta P}{P_0}\right) - (1-\psi)\tan\emptyset \tag{55}$$

The relation between reactive power mismatch ($\Delta Q/P$) and real power mismatch ($\Delta P/P$) is illustrated by straight line with a slope equal to ($\psi * \tan\Phi$). The non-detection zone is drawn from the threshold limit of TAU. TAU varies from 0° to 1° for normal operation. The PSI ranges from 0.9994 to 1 in normal operating conditions. So NDZ is bounded by two straight lines such as balanced boundary and unbalanced boundary lines. The symmetrical and unsymmetrical boundary equations are expressed in Equations (56) and (57). The balanced boundary line moves through the origin.

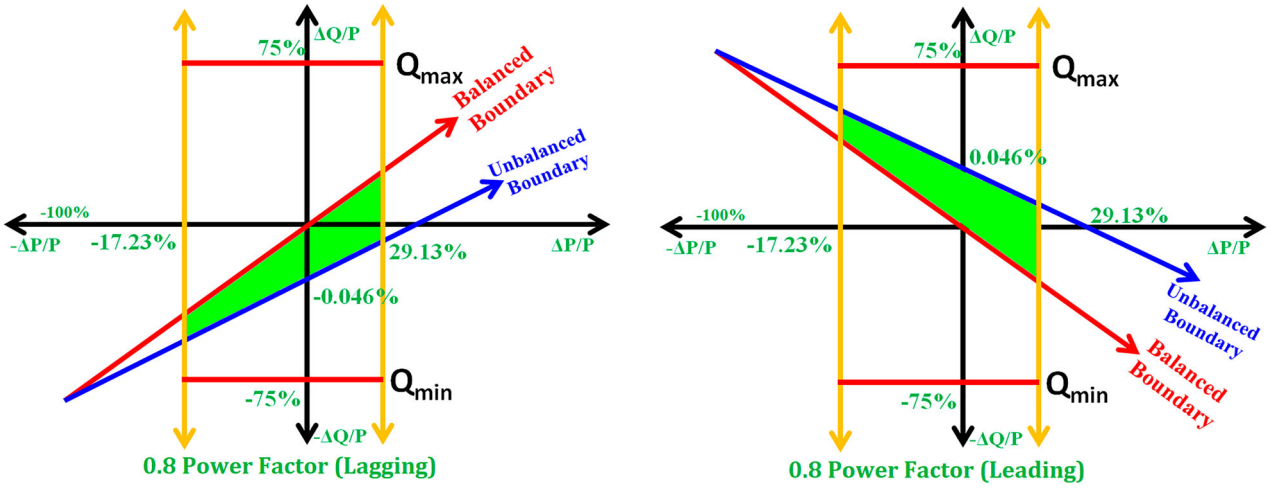

Figure 9. NDZ of ASCOV relay.

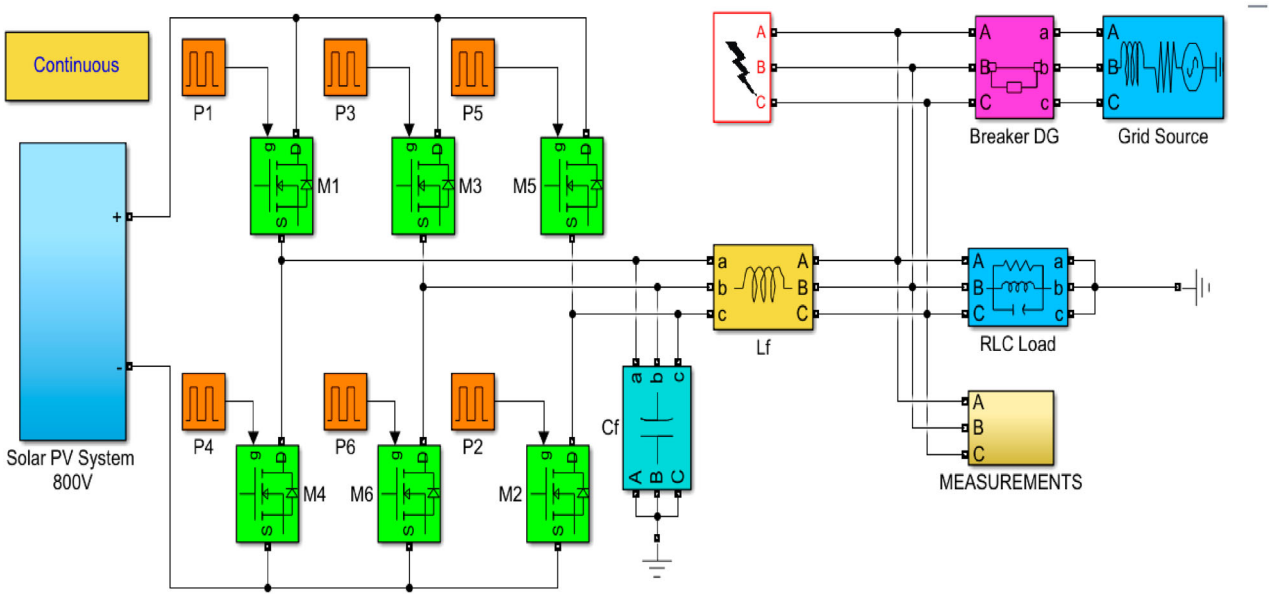

Figure 10. Simulation diagram of solar-powered microgrid.

These boundary lines intersect each other at a point (−1, –tanΦ). There is no boundary for unity power factor (tan Φ = 0).

$$\left(\frac{\Delta Q}{P_0}\right)_{bal} = \tan \emptyset \left(\frac{\Delta P}{P_0}\right)_{bal} \tag{56}$$

$$\left(\frac{\Delta Q}{P_0}\right)_{unb} = \psi_0 \tan \emptyset \left(\frac{\Delta P}{P_0}\right)_{unb} - (1-\psi_0)\tan \emptyset \tag{57}$$

We consider the power factor variations from 0.8 (lag) and 0.8 (lead). The value of Tan Φ is negative for leading power factor and positive for lagging power factor.

Area of OUV/OUF relay

$$= (P_{\max} - P_{\min}) * (Q_{\max} - Q_{\min})$$

Area of ASCOV relay

$$= (1-\psi_0)\tan \Phi * (P_{\max}^2 - P_{\min}^2)/2$$

Table 2. System parameters.

Parameters	Ratings
Solar irradiance	1000
Operating Temp	25°C
DC Voltage	800 V
Filter Inductance and Capacitance	3.8 mH, 0.0027 F
Grid voltage	400 Vrms (ph-ph)
Grid resistance	0.01 Ω
Grid Inductance	0.3 mH
Load Parameters	R = 18.15 Ω L = 23.109 mH C = 438 μ F

Figure 11. (i) Line voltages (AB and BC), (ii) RMS of line voltages, (iii) Angle between two-line voltages, (iv) LARMS voltage, (v) PSI, (vi) TAU, trip signals generated by (vii) OUV/OUF relay, (viii) ROCOF relay, (ix) VUTHD relay and (x) Proposed ASCOV relay during the grid-connected mode.

$= 3 \tan \Phi * (P_{max}^2 - P_{min}^2) \times 10^{-4}$

Area of ASCOV relay/Area of OUV - OUF relay

$= 3 \tan \Phi (P_{max} + P_{min})/(Q_{max} - Q_{min}) \times 10^{-4}$

Area of ASCOV relay/Area of OUV - OUF relay

$= 0.05 * \tan \Phi \ \%$

If Tan $\Phi = 0.75$, then the NDZ Area of the proposed relay is about 0.0375% of the NDZ Area of OUV/OUF Relay.

Lagging Power factor:

Origin of Lines: $(-1,-0.75)$

Y -axis vertex in unbalanced boundary line $= -0.4658 \times 10^{-3}$

Leading Power factor:

Origin of Lines: $(-1, 0.75)$

Y -axis vertex in unbalanced boundary line $= 0.4658 \times 10^{-3}$

X -axis vertex (All Power factors excluding unity) $= \psi/(1-\psi) = 1640.57$

Non-detection zone of ASCOV relay is shown in Figure 9 for leading and lagging power factors. The diagram has been drawn for the fixed power factor. But practically, power factor also changes during islanding events. So the anti-islanding performed by PSI works in the zero power mismatches. Red line and blue line in the figure denote the balance boundary line and unbalanced boundary line, respectively. The region bounded

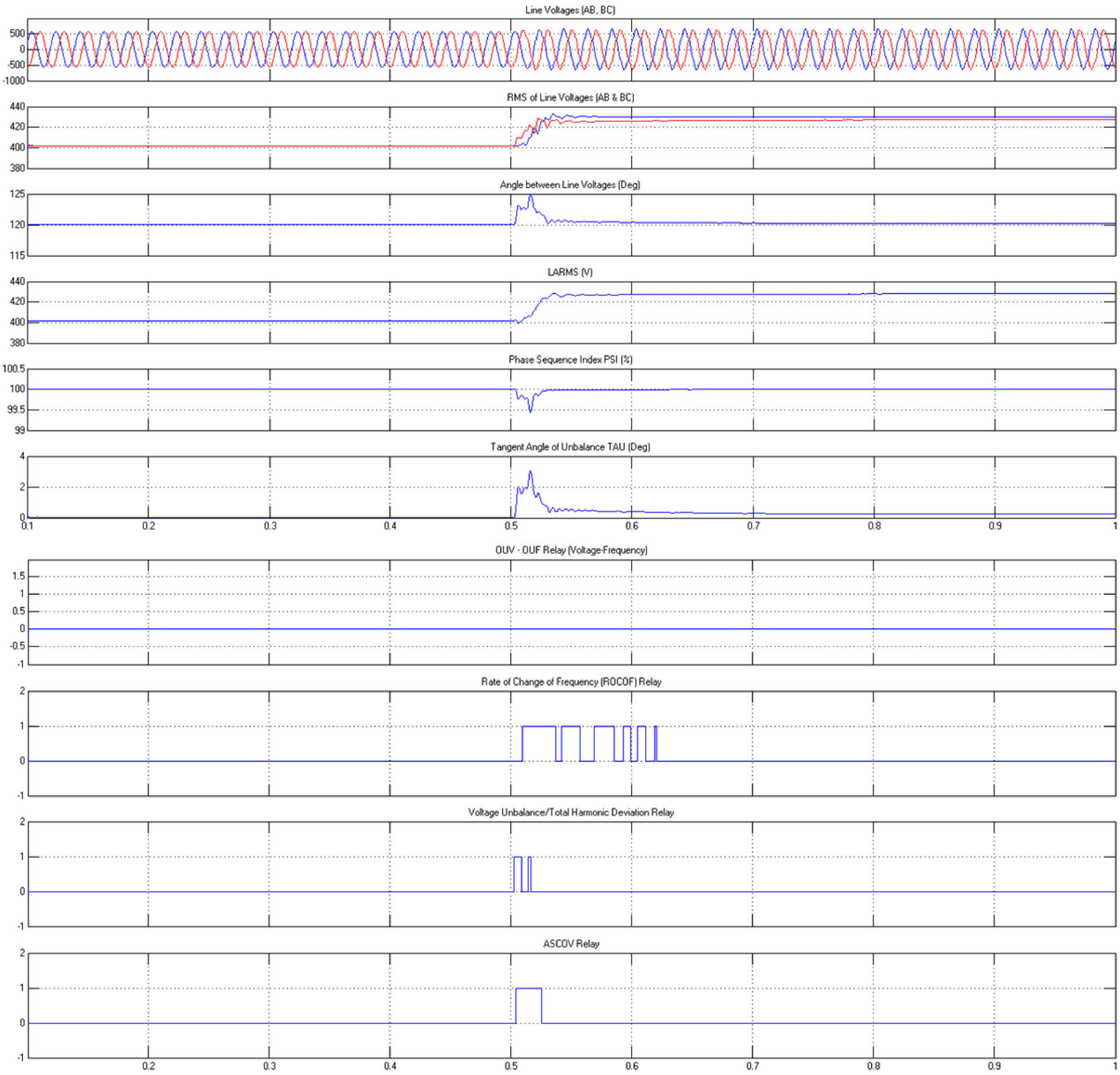

Figure 12. (i) Line voltages (AB and BC), (ii) RMS of line voltages, (iii) Angle between two-line voltages, (iv) LARMS voltage, (v) PSI, (vi) TAU, trip signals generated by (vii) OUV/OUF relay, (viii) ROCOF relay, (ix) VUTHD relay and (x) Proposed ASCOV relay during islanding detection test at 0.5 s.

by these boundary lines is shaded with green denotes the non-detection zone of angle relay. NDZ of magnitude relay is bounded by two yellow lines. This region is very small compared to the NDZ of existing relays.

4. Result and discussion

In this manuscript, a novel ASCOV relay is proposed for identifying the condition of islanding with LARMS voltage and TAU. The TAU provides the voltage unbalance and phase angle shift. Anti-islanding trip signal is generated by comparing LARMS voltage and TAU with its thresholds. During non-islanding conditions like nonlinear load switching and load switching, no trip signal is produced using this proposed approach. Besides, the ASCOV relay does not affect the power system quality as it not only disturbs any disturbance signals. The proposed model is executed on MATLAB/Simulink working stage and PV-based inverter-connected distribution system modelling is shown in Figure 10.

The solar panel produces the 800 V constant voltage to the inverter. The inverter is intended with six MOSFETs which are associated in three arms. For converting the DC supply into a 50-Hz AC supply, the standard pulses are provided. Moreover, the inductive-capacitive filter is utilized for eliminating the ripples produced via the inverter. The parallel RLC load is linked with DG for simulating the islanding as per the standard of IEEE [33,34]. In parallel RLC load, anti-islanding procedure of the proposed approach for various quality factors Q_f, reactive power Q and real power P is simulated. Besides, the supply of the grid is modelled with a three-phase generator with series inductance and resistance [26].

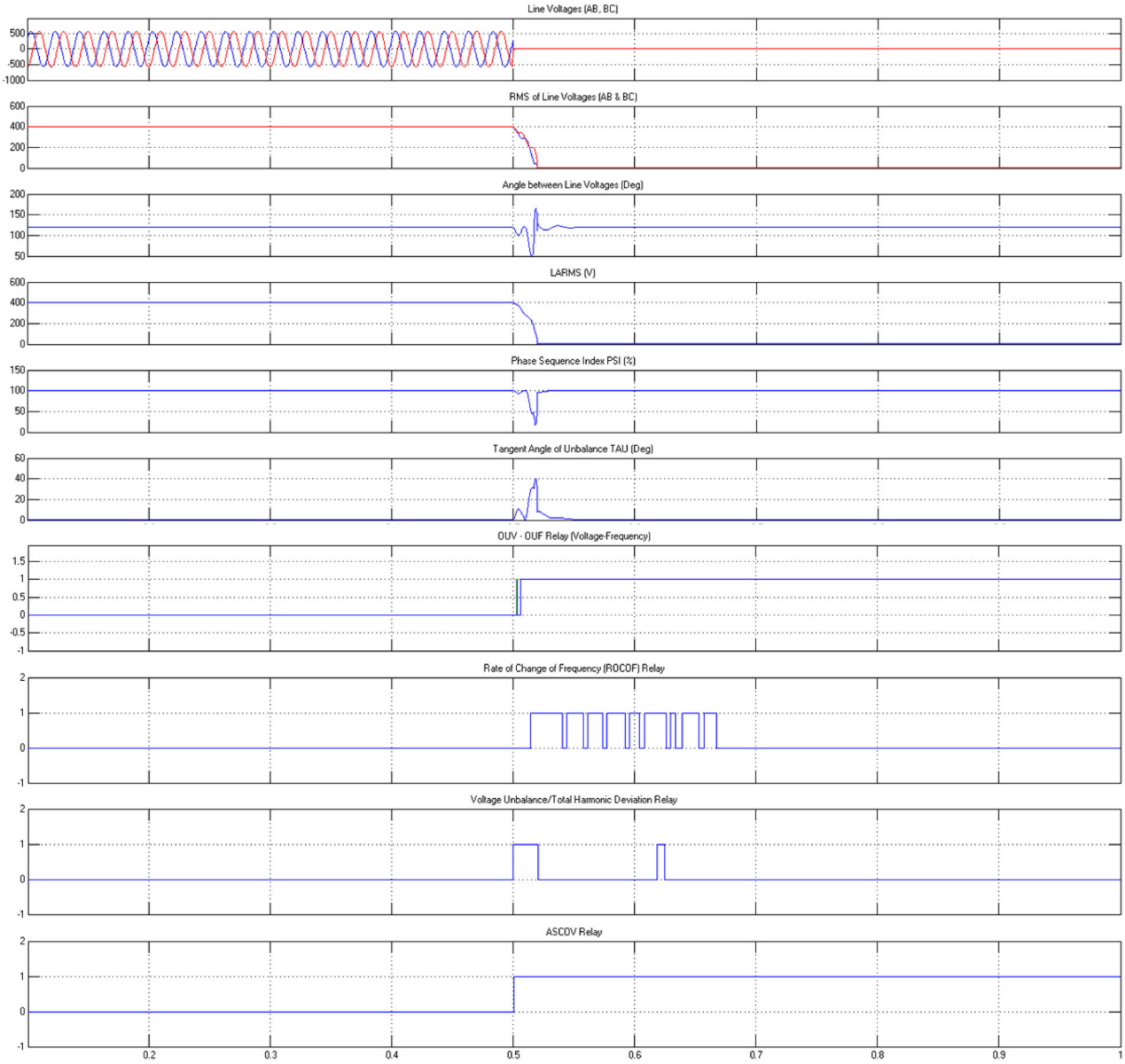

Figure 13. (i) Line voltages (AB and BC), (ii) RMS of line voltages, (iii) Angle between two-line voltages, (iv) LARMS voltage, (v) PSI, (vi) TAU, trip signals generated by (vii) OUV/OUF relay, (viii) ROCOF relay, (ix) VUTHD relay and (x) Proposed ASCOV relay during symmetrical fault test at 0.5 s.

The parameters utilized for simulations are displayed in Table 2.

In this paper, the filter inductance and capacitance values are taken as 3.8 mH, 0.0027 F. The value of grid Voltage and DC Voltage is taken as 400 Vrms (ph-ph) and 800 V. The value of the grid resistance is 0.01 Ω and the inductance of the grid is 0.3 mH. The method is validated with various islanding conditions, symmetrical and unsymmetrical faults. The achieved outcomes are compared with conventional islanding detection methods such as Overvoltage/Undervoltage (OUV), Overfrequency/Underfrequency (OUF), Rate of Change of Frequency (ROCOF), Voltage Unbalance and Total Harmonic Distortion (VUTHD) etc.., for evaluating the proposed approach effectiveness.

4.1. Case 1: grid-connected mode

In the grid-connected mode, parallel RLC load is powered through the utility grid and distributed generation system. The breaker remains in the closed position. The simulation provides the signals in normal state. Furthermore, the entire simulation time is taken as 1 s. The microgrid system simulated at a grid-connected mode is demonstrated in Figure 11. Line voltage signals and their parameters, and ASCOV parameters such as LARMS voltage, PSI and TAU are shown in Figure 11. The two-line voltages (AB and BC) are shown instead of three-line voltages. Third-line voltage can be obtained using other two-line voltages. RMS values of the line voltages are measured as 401.7 V and 401.5 V, respectively. It gives the LARMS voltage of 401.6 V. Tangent angle of unbalance is estimated as 0.016° (nearly zero)

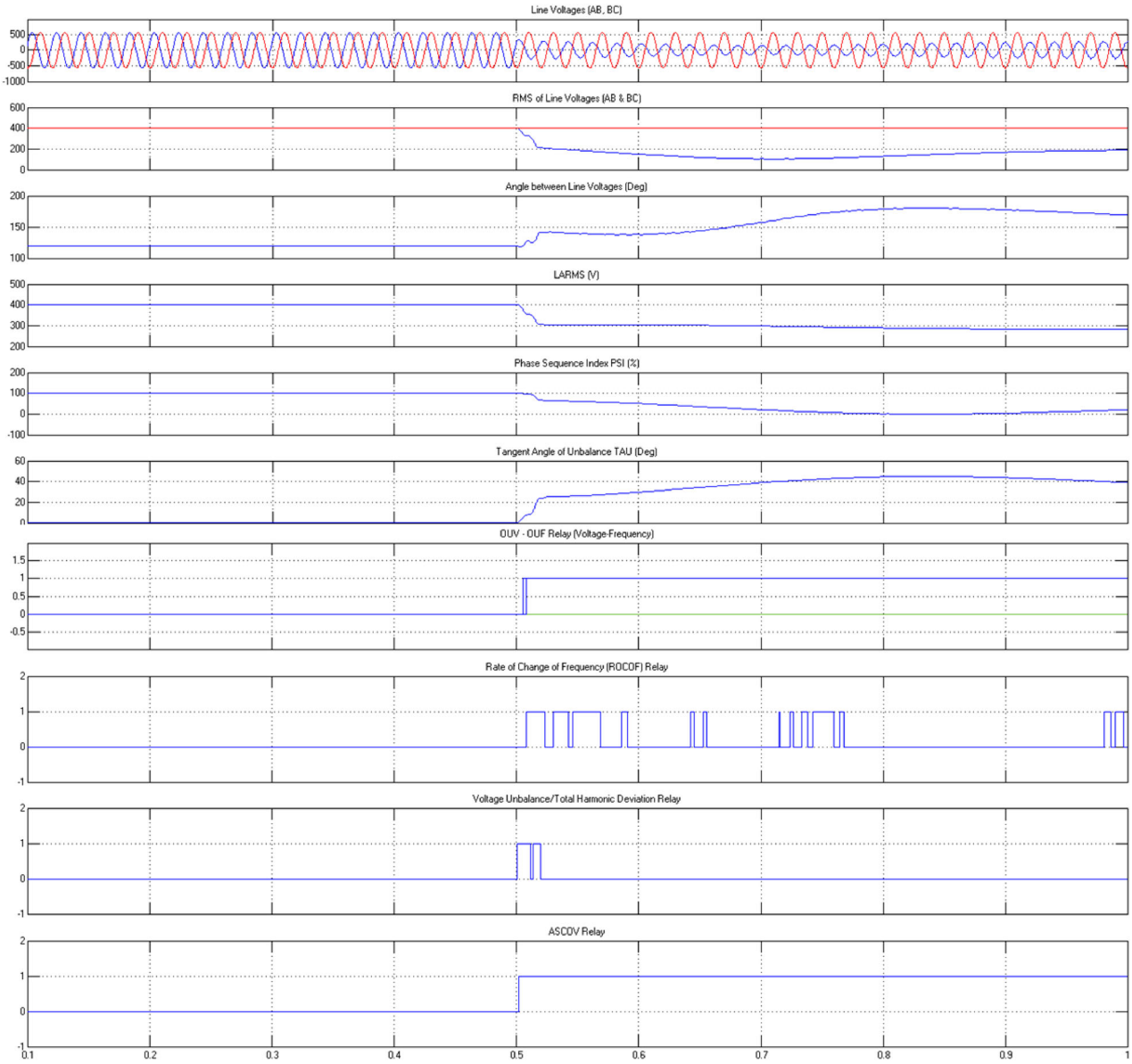

Figure 14. (i) Line voltages (AB and BC), (ii) RMS of line voltages, (iii) Angle between two-line voltages, (iv) LARMS voltage, (v) PSI, (vi) TAU, trip signals generated by (vii) OUV/OUF relay, (viii) ROCOF relay, (ix) VUTHD relay and (x) Proposed ASCOV relay during unsymmetrical fault test (single line to ground fault) at 0.5 s.

for 120° phase angle between the line voltages in normal condition. Phase Sequence Index indicates 100%.

The trip signals generated by conventional relays and the proposed ASCOV relay are indicated in Figure 11. Overvoltage/Undervoltage (OUV) relay compares the RMS value of three-line voltages with the range of 352 V (88%)−440 V (110%) as per IEEE Standard. Over-frequency/underfrequency (OUF) relay compares the frequency of supply between 49.5Hz and 50.2Hz. The threshold for the ROCOF relay has been fixed as 2.5 Hz/s. VUTHD relay consists of two sub-relays. Voltage Unbalance Deviation is checked with the limits between −100% and +50%. The THD Threshold limit is fixed as 100%. ASCOV relay consists two relays such as magnitude relay which is identical to OUV relay and angle relay which compares the TAU with the range of 0°–1°. Voltage Unbalance factor ranges from 0% to infinity whereas TAU ranges between 0° and 90° which is nearly equivalent to percentage. All relays do not generate trip signal during normal condition.

4.2. Case 2: islanding mode

For estimating the proposed ASCOV relay performance, the anti-islanding test is conducted. Here, the Islanding is performed by disconnecting the utility grid from load through the breaker. The opening time of the breaker is set as 0.5 s. During this test, the transients will occur at the circuit breaker opening time. Due to this, it generates the unbalance of the voltage for little interval. The obtained simulation outcome after the execution is denoted in Figure 12. The RMS value of line voltage between phases "A" and "B" is increased up to 433.14 V and then decreased to 429.5 V as steady state. Line

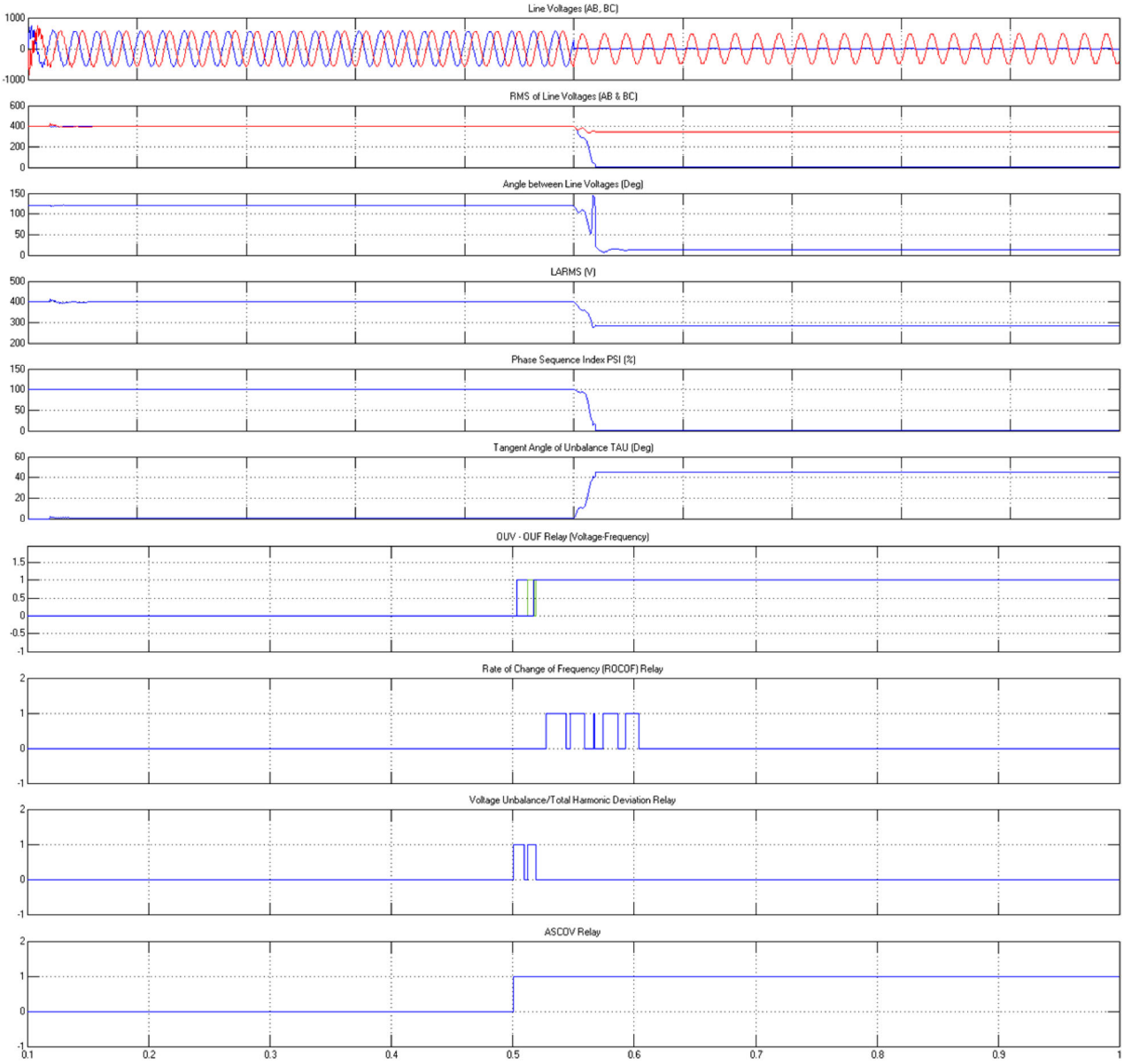

Figure 15. (i) Line voltages (AB and BC), (ii) RMS of line voltages, (iii) Angle between two-line voltages, (iv) LARMS voltage, (v) PSI, (vi) TAU, trip signals generated by (vii) OUV/OUF relay, (viii) ROCOF relay, (ix) VUTHD relay and (x) Proposed ASCOV relay during unsymmetrical fault test (double line faults: A–B) at 0.5 s.

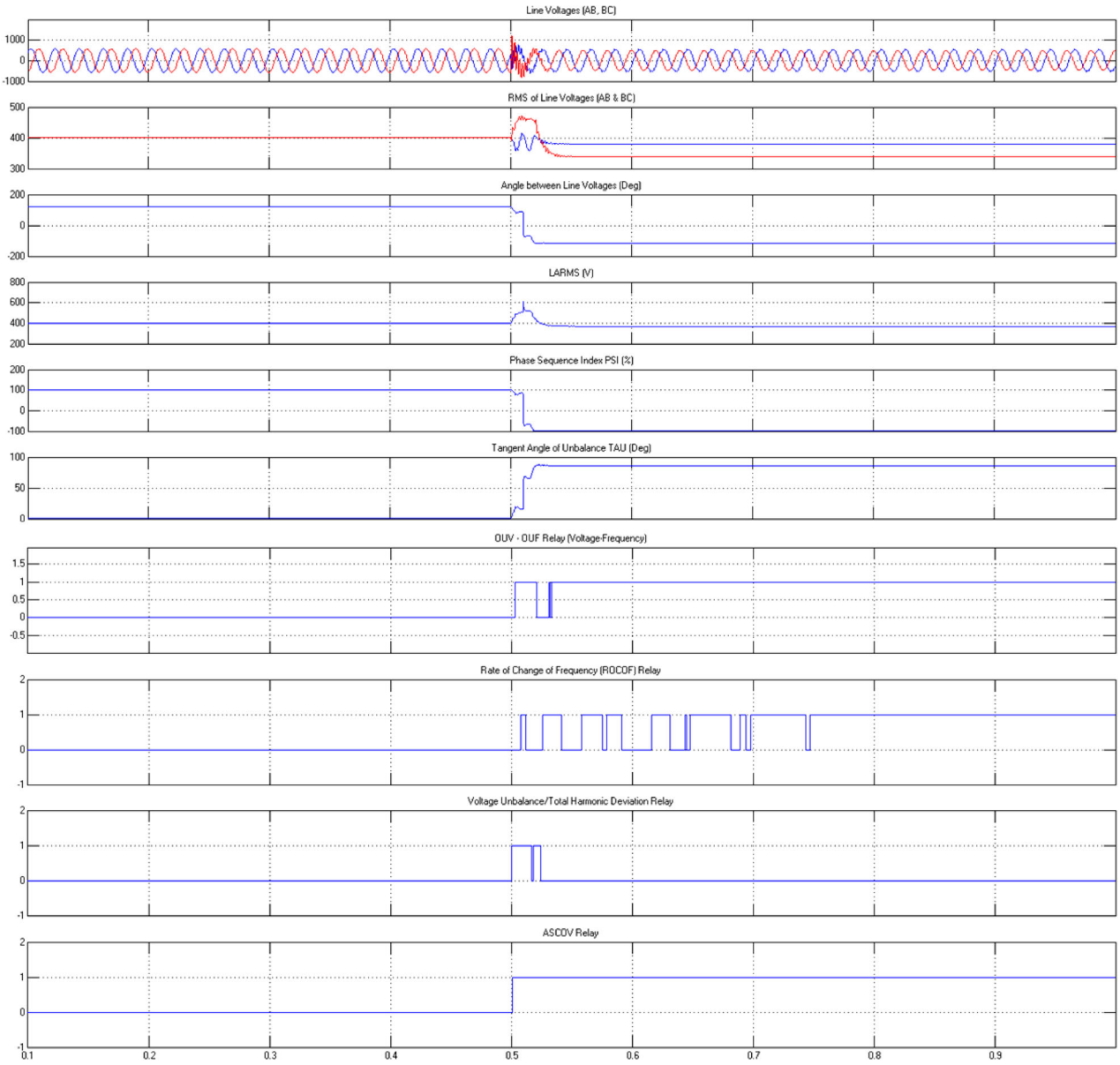

Figure 16. (i) Line voltages (AB and BC), (ii) RMS of line voltages, (iii) Angle between two-line voltages, (iv) LARMS voltage, (v) PSI, (vi) TAU, Trip signals generated by (vii) OUV/OUF relay, (viii) ROCOF relay, (ix) VUTHD relay and (x) Proposed ASCOV relay during phase reversal (B & C) at 0.5 s.

Table 3. ASCOV parameters for various islanding and non-islanding events.

Case	Description	RMS (V_{ab})	RMS (V_{bc})	Phase Angle (Deg)	LARMS voltage (V_λ)	TAU (Deg)	PSI (%)	VUF Tan(Tau) (%)
1	Normal	401.7	401.5	120	401.6	0.016	100	0.028
2	Islanding detection (peak)	433.14	428.4	124.86	428.6	3	99.44	5.24
3	Symmetrical Fault Three Phase	4.482	4.482	165 (peak)	4.482	40	17	83.91
4	Unsymmetrical Faults: Single Line to Ground A-G	187.2	400.5	169	285	39.13	20.34	81.38
	B-G	219.9	187.2	20.33	285.2	39.14	20.3	81.35
	C-G	400.7	219.9	170.7	285.1	39.15	20.29	81.41
5	Unsymmetrical Faults:Double Line A-B	4.5	344.4	13.31	283	44.85	0.51	99.48
	B-C	348.8	4.5	167	283	44.85	0.51	99.48
	C-A	344.4	348.8	179.8	283	44.85	0.52	99.48
6	Phase Shifting	380.3	338.9	114.9	369.8	85.32	−98.67	1221.5
7	Linear Load Switching	403.7	403.3	403.5	120	0.034	100	0.06
8	Nonlinear Load Switching	403	402.8	402.9	120	0.012	100	0.02

voltage RMS between phases “B” and “C” is increased up to 428.42 V and then decreased to 427.2 V. These voltages are lesser than 440 V (110%), so the OUV relay does not trigger the signal and hence islanding. Phase angles between line voltages are shifted from 120° to 124.86°, then it decreased to 120.2°. Maximum Values

of LARMS voltage and TAU are 428.6 V, 3°, respectively. PSI is decreased up to a minimum value of 99.44%, then it comes to 100%. Signal variations are indicated in Figure 12. Phase Angle variations and TAU clearly indicate the state of unbalance.

Trip signal generated by various relays has been shown in Figure 12. Detection time of ROCOF relay, VUTHD relay and ASCOV relay are 509.8, 502.6 and 504.2 ms, respectively. If we reduce the threshold for TAU from 1° to 0.5°, then detection time will be reduced to 503.7 ms.

4.3. Case 3: symmetrical fault detection test

Solar-powered distributed generation is protected against faults by islanding condition. The anti-islanding methods should detect the fault condition as soon as possible to trip the breaker. So fault test has to be conducted to validate the anti-islanding method. Three phase to ground fault is initiated at 0.5 s. Line voltage and ASCOV parameters under symmetrical fault condition are shown in Figure 13. RMS values of two-line voltages and LARMS voltage are reduced to 4.482 V. Phase angle oscillates between 50° and 165° for a period of 25 ms. Phase angle value after the occurrence of fault is 120°. So the system is observed as in balanced condition after the three-phase fault. Small unbalance condition for the short period creates an islanding situation. Minimum value of PSI and maximum value of TAU are measured as 17% and 40°, respectively. All relays trigger the trip signal. Detection time of trip signal for OUV/OUF relay, ROCOF relay VUTHD relay and ASCOV relay are 503.1, 514.9, 500.1 and 500.5 ms, respectively, as shown in Figure 13. ROCOF relay generates more pulsating trip signals.

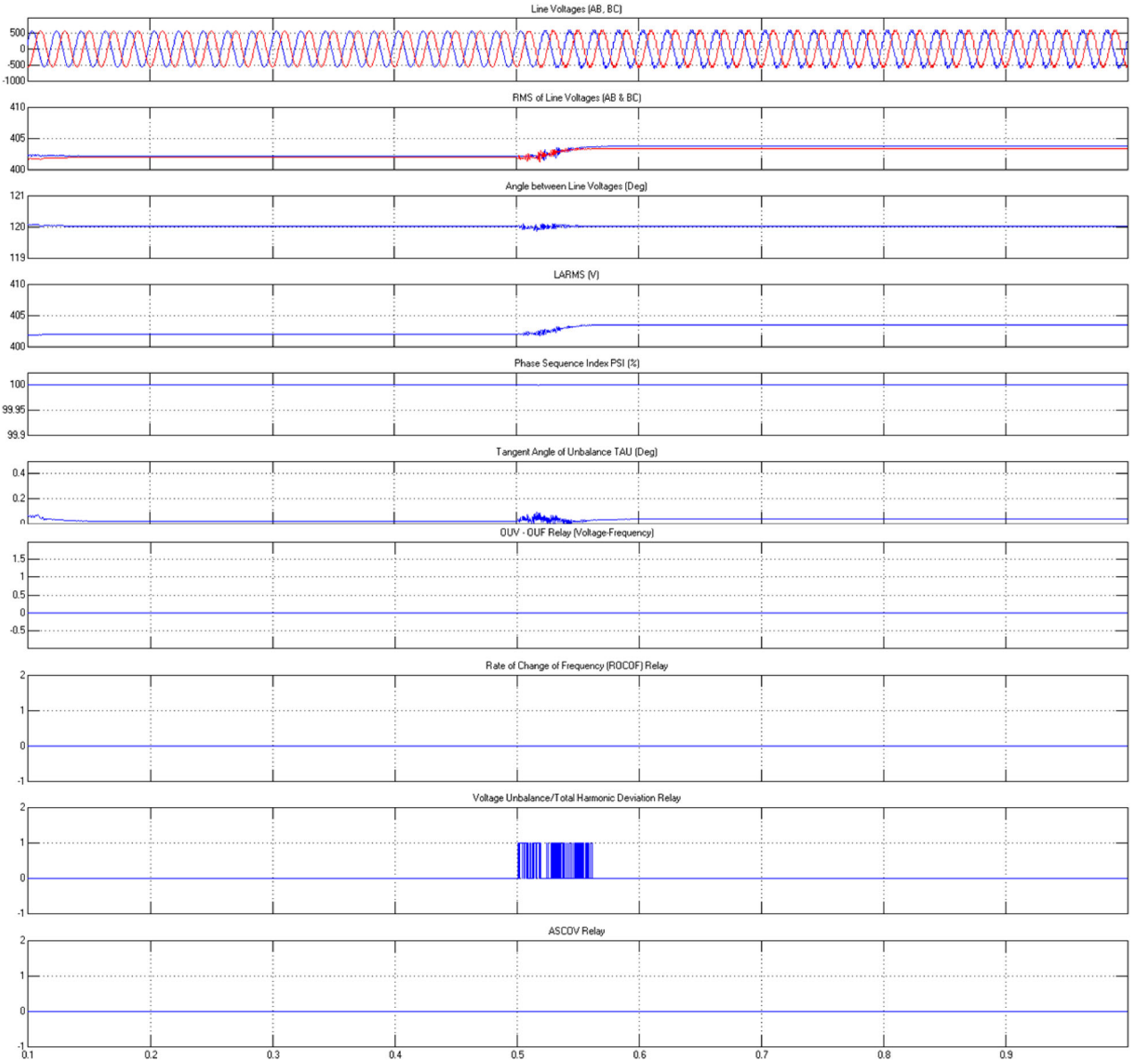

Figure 17. (i) Line voltages (AB and BC), (ii) RMS of line voltages, (iii) Angle between two-line voltages, (iv) LARMS voltage, (v) PSI, (vi) TAU, Trip signals generated by (vii) OUV/OUF relay, (viii) ROCOF relay, (ix) VUTHD relay and (x) Proposed ASCOV relay during half load switching at 0.5 s.

4.4. Case 4: unsymmetrical fault detection test: single line to ground

Symmetrical components are mainly used for unbalanced fault analysis. So the proposed method is tested to various unsymmetrical faults. Single line to ground fault is initiated in phase "A" at 0.5 s. Phase "A" Voltage will be reduced nearly to zero for a single line to ground fault. Line voltage between B and C is not affected and the rms value is measured as 400.5 V. Line Voltage between phases "A" and "B" is reduced to 187.2 V (rms). LARMS Voltage and PSI are decreased to 285 V and 20.34%. Phase angle is increase to 169°. The tangent angle of unbalance is increased to 39.13°. All signals with respect to a single line to ground fault are displayed in Figure 14. All relays respond to this fault and generate the trip signals which are displayed in Figure 14. Detection times of various relays are displayed in Table 4.

4.5. Case 5: unsymmetrical fault detection test: double line faults

Double Line faults are tested following the single line to ground fault test. Phases A and B are short-circuited to initiate line fault. So the Line voltage AB is reduced to 4.5 V (nearly to zero) whereas the Line voltage BC is slightly reduced to 344.4 V as shown in Figure 15. Reduced values of Phase angle, LARMS voltage and PSI are 13.31°, 283 V and 0.51%, respectively. TAU is increased to 44.85%. Detection times of all relays are tabulated in Table 4.

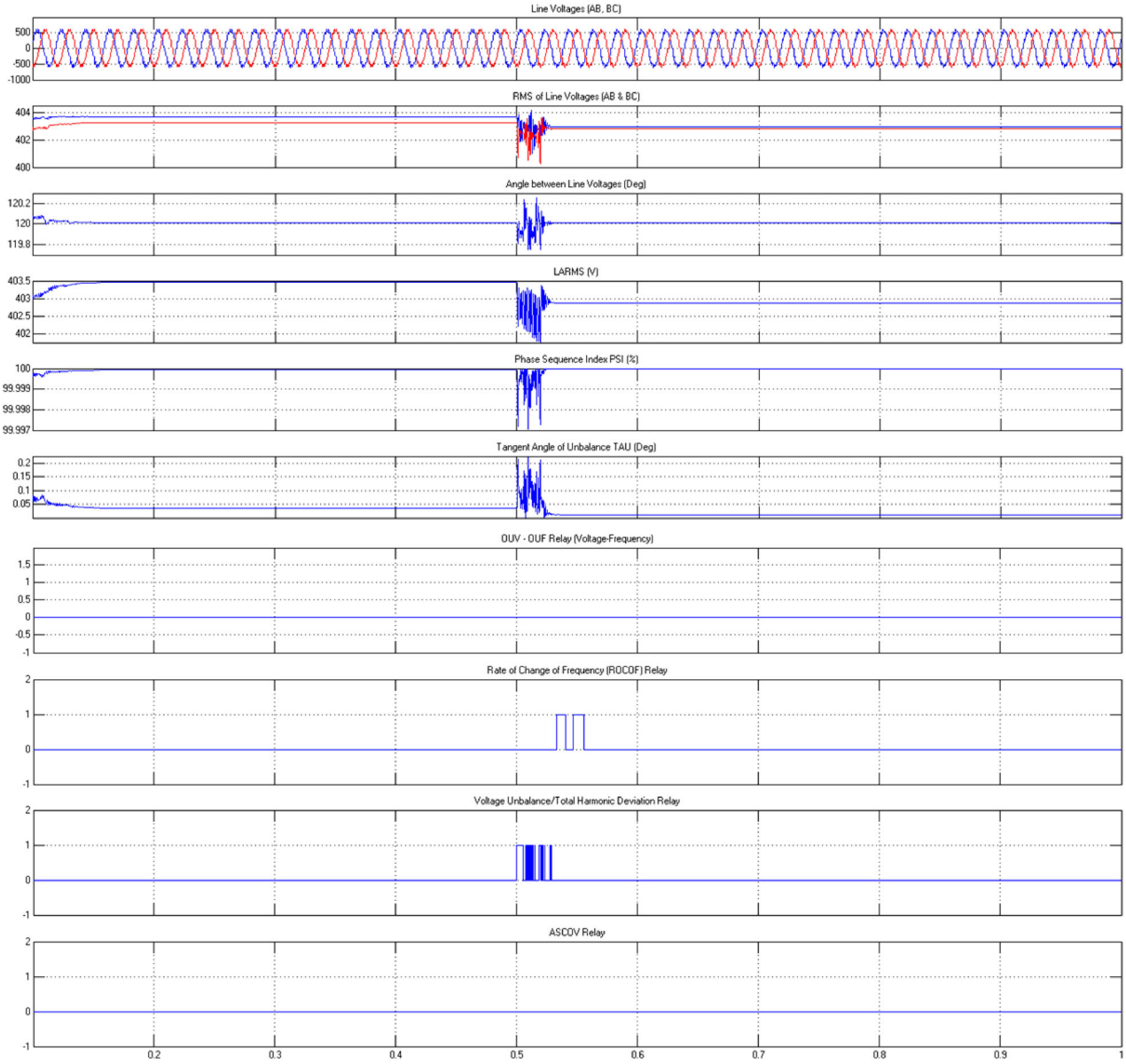

Figure 18. (i) Line voltages (AB and BC), (ii) RMS of line voltages, (iii) Angle between two-line voltages, (iv) LARMS voltage, (v) PSI, (vi) TAU, trip signals generated by (vii) OUV/OUF relay, (viii) ROCOF relay, (ix) VUTHD relay and (x) Proposed ASCOV relay during nonlinear load switching at 0.5 s.

4.6. Case 6: phase shifting

Islanding detection is performed by detecting the state of unbalance. Phase reversal will also create the unbalance of system. So islanding detection test has been performed during phase reversal test. Phases B and C are interchanged at 0.5 s. RMS of line voltages are decreased after small oscillations to 380.3 V and 338.9 V, respectively. Phase angle is decreased to −114.9° (nearly to −120°) due to phase reversal. LARMS voltage and TAU are observed after phase reversal as 369.8 V and −98.67%, respectively. Tau is increased to 85.32°. All relays generates the trip signal as shown in Figure 16, with different timings as listed in Table 3.

4.7. Case 7: linear load switching

Voltage and frequency relays fails to detect the fault in low power mismatches. Angle relay is more sensitive compared to voltage and frequency relays. So it is easily detects the fault conditions. But Anti-islanding should not process during the internal faults like load switching, nonlinear load switching etc. So proposed relay does not generate trip signal during these internal faults which are referred as non-islanding events. Linear load switching test is conducted by disconnecting 50% of the load after 0.5 s. Short oscillations with duration of 60 ms are observed during load switching condition as shown in Figure 17(a). RMS of line voltages and LARMS Voltage after load switching are measured as 403.7, 403.3 and 403.5 V, respectively. Phase angle and PSI remains at 120° and 100%, respectively. TAU slightly increased to 0.034°. So unbalance is not created during load switching conditions. VUTHD relay only creates trip signals compared to other relay as shown in Figure 17.

4.8. Case 8: nonlinear load switching

Nonlinear load creates the harmonics which will vary the voltage levels. So the nonlinear load test is conducted to test the islanding process against the harmonics. These variations are very small compared to surges, so that the relay must not trigger the signal. A nonlinear load test is conducted by connecting the three-phase bridge rectifier with a resistive load at 0.5 s. Line Voltages variation under this test is negligible as shown in Figure 18. RMS and frequency variation is very small. Short oscillations with a duration of 60 ms are observed during load switching condition as shown in Figure 18(a). RMS of line voltages and LARMS Voltage after load switching are measured as 403 V, 402.8 V and 402.9 V, respectively. Phase angle and PSI remains at 120° and 100%, respectively. TAU slightly increased to 0.012°. So unbalance is not created during load switching conditions. The ROCOF and VUTHD relay generate a trip signal as shown in Figure 18.

Magnitudes of two-line voltages and phase angle between them are tabulated in Table 3 under different fault conditions. LARMS Voltage and Tangent Angle of Unbalance are also measured in simulation. The tangent of TAU gives the Voltage Unbalance Factor.

Table 4 gives the detection time of various relays such as OUV/OUF, ROCOF and VUTHD, and compared

Table 4. Comparison of relays with detection time (fault time: 0.5 s).

		Detection time (ms) (Td-0.5)∗1000			
Case	Description	OUV/OUF	ROCOF	VUTHD	ASCOV
1	Normal	–	–	–	–
2	Islanding detection (peak)	–	9.8	2.6	2.4
3	Symmetrical Fault Three Phase	3.1	14.9	0.1	0.5
4	Unsymmetrical Faults: Single Line to Ground A-G	4.9	7.8	4.5	1.9
	B-G	3.9	25	0.1	0.6
	C-G	8	25	0.1	0.9
5	Unsymmetrical Faults: Double Line A-B	3.3	27.4	0.1	0.7
	B-C	3.2	7.7	0.1	0.6
	C-A	6.4	28.8	0.1	1
6	Phase Shifting	3.1	8.1	0.1	0.5
7	Linear Load Switching	–	–	0.7	–
8	Nonlinear Load Switching	–	32.8	0.2	–

Table 5. Comparison of voltage unbalance factors under various definitions for symmetrical and unsymmetrical faults.

SI No	Faults	Actual VU (%)	IEEE1 (%)	IEEE2 (%)	NEMA (%)	PAM (%)	CIGRE (%)	Proposed method (%)
1	Three-Phase Fault	0.01485	0.01295 (12.79)	0.025 (68.35)	0.01295 (12.79)	0.01456 (1.95)	0.0145 (2.35)	0.01461 (1.62)
2	A-G	81.37	73.84 (9.25)	124.6 (53.13)	48.79 (40)	49.5 (39.17)	81.19 (0.22)	81.36 (0.01)
3	B-G	81.39	73.87 (9.24)	124.6 (53.09)	48.8 (40.04)	49.51 (39.17)	81.23 (0.19)	81.39 (0)
4	C-G	81.41	73.76 (9.39)	124.6 (53.05)	48.8 (40.05)	49.51 (39.18)	81.24 (0.21)	81.41 (0)
5	A-B	99.49	50 (49.74)	76.42 (23.19)	98.07 (1.43)	98.49 (1)	99.48 (0.01)	99.49 (0)
6	B-C	99.49	50 (49.74)	76.42 (23.19)	98.07 (1.43)	98.49 (1)	99.48 (0.01)	99.49 (0)
7	C-A	99.48	50 (49.74)	76.42 (23.19)	98.07 (1.43)	98.49 (1)	99.48 (0.01)	99.49 (0)
8	A-B-G	96.15	41.18 (57.17)	63.07 (34.4)	95.95 (0.21)	96.37 (0.23)	96.15 (0)	96.15 (0)
9	B-C-G	96.12	40.05 (58.33)	61.38 (36.14)	95.92 (0.21)	96.34 (0.23)	96.12 (0)	96.12 (0)
10	C-A-G	96.15	40.44 (57.94)	61.95 (35.57)	95.93 (0.23)	96.35 (0.21)	96.15 (0)	96.15 (0)
11	Phase reversal	1236	7.915 (99.36)	13.1 (98.94)	8.234 (99.33)	8.373 (99.32)	8.21 (99.36)	1223 (1.05)

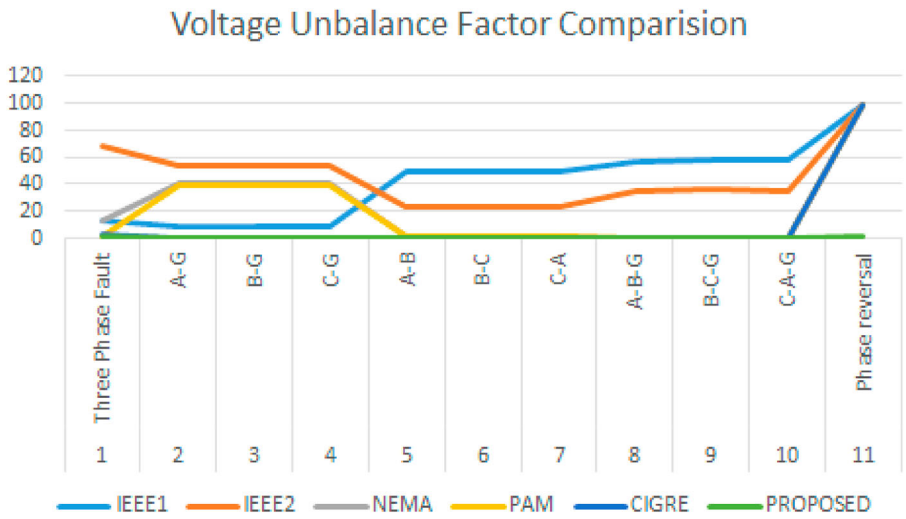

Figure 19. Errors (%) of voltage unbalance factor by various methods.

Table 6. Comparison of the proposed method with other method in terms of accuracy.

References	Year	Methods	Advantages/Drawbacks	Accuracy (%)
Vyas et al. [25]	2017	Data analytics and computational methods	A mismatch between the load and lower accuracy for detection	97.42
Salimi et al. [35]	2019	variational mode decomposition	Large detection errors	98.7
Bhatt et al. [24]	2020	Modal Current and Adaptive Boosting	Higher cost	97.98
Reddy et al. [23]	2020	Random Forest and Moth Flame Optimization (RFMFO)	Higher detection time	98.5
Proposed method	2022	Proposed Anti-Islanding ASCOV Relay for Photovoltaic Inverter-Based Distributed Generation	Better recall and precision, less computation and reduces the complexity of the algorithm	99

with the ASCOV relay. ASCOV relay clearly separates islanding events with non-islanding events.

Voltage unbalance factors for symmetrical faults, unsymmetrical faults and phase reversal conditions are determined using simulation. Faults are created at 0.5 s. Values shown in Table 5 are taken at the time of 1 s. Errors are shown inside the brackets for comparison. Voltage Unbalance factors under NEMA, IEEE and PAM definitions differ from the original value for unbalanced fault conditions. Voltage unbalance factor by CIGRE definition is closely equal to the actual value for all fault conditions excluding phase reversals. In phase reversal conditions, the proposed method gives the most accurate value. Errors of VUF which are determined by various methods are illustrated in Figure 19 and Table 6.

5. Conclusion

In this paper, a novel Angular symmetrical components-based Islanding Detection technique is proposed. The proposed technique clearly identifies the condition of islanding with two parameters namely LARMS voltage and Tangent Angle of Unbalance respectively. The proposed relay does not trigger non-islanding events like linear load switching and non-linear load switching. The proposed method does not affect the power quality. Voltage Unbalance Factor estimated using this method is most accurate compared to other method. Magnitudes of symmetrical components can be estimated using the line voltage parameters without the help of a sequence analyser. Tangent Angle of Unbalance and Phase Sequence Index are the new parameters to analyse various unbalance conditions. The relay works even in zero power mismatches with negligible Non-Detection Zone. Furthermore, the proposed ASCOV relay is executed in MATLAB/Simulink and the execution was assessed with the other solution techniques. Consequently, the outcome indicates that proposed efficiently identifies the islanding condition with better recall and precision, less computation and reduces the complexity of the algorithm with the accuracy of 99%.

Disclosure statement

No potential conflict of interest was reported by the author(s).

References

[1] Blaabjerg F, Consoli A, Ferreira JA, et al. The future of electronic power processing and conversion. IEEE Trans Power Electron. May 2005;20(3):715–720.
[2] IEEE recommended practice for utility interface of photovoltaic (PV) systems. IEEE Std. 929, Standards Coordinating Committee 21 on Photovoltaics, New York (NY), Apr. 2000.
[3] IEEE standard for interconnecting distributed resources with electric power systems, IEEE Std. 1547, 2003.
[4] Blaabjerg F, Teodorescu R, Liserre M, et al. Overview of control and grid synchronization for distributed power

generation systems. IEEE Trans Ind Electron. October 2006;53(5):1398–1409.
[5] Zheng T, Yang H, Zhao R, et al. Design, evaluation and implementation of an islanding detection method for a micro-grid. Energies. 2018;11:323.
[6] Rami Reddy C, Harinadha Reddy K. Islanding detection techniques for grid integrated distributed generation – a review. Int J Renew Energy Res. June 2019;9(2):960–977.
[7] Ropp ME, Aaker K, Haigh J, et al. Using power line carrier communications to prevent islanding [of PV power systems]. Conference Record of the Twenty-Eighth IEEE Photovoltaic Specialists Conference; Sept. 15–22; 2000. pp. 1675–1678.
[8] Zeineldin HH, Kirtley J. Performance of the OVP/UVP and OFP/UFP method with voltage and frequency dependent loads. IEEE Trans Power Delivery. Apr. 2009;24(2):772–778.
[9] Reddy CR, Reddy KH. Islanding detection method for inverter based distributed generation based on combined changes of ROCOAP and ROCORP. Int J Pure Appl Math. 2017;117(19):433–440.
[10] Vieira JCM, Freitas W, Huang Z, et al. Formulas for predicting the dynamic performance of ROCOF relays for embedded generation applications. IEE Proc Gener Transm Distrib. July 2006;153(4):399–406.
[11] Dutta S, Sadhu PK, Reddy MJB, et al. Shifting of research trends in islanding detection method – a comprehensive survey. Prot Control Mod Power Syst. 2018;3(1):1–20.
[12] Jang S-I, Kim K-H. An islanding detection method for distributed generations using voltage unbalance and total harmonic distortion of current. IEEE Trans Power Delivery. Apr. 2004;19(2):745–752.
[13] Ropp ME, Begovic M, Rohatgi A. Analysis and performance assessment of the active frequency drift method of islanding prevention. IEEE Trans Energy Convers. Sept. 1999;14(3):810–816.
[14] Zeineldin HH, Kennedy S. Sandia frequency-shift parameter selection to eliminate nondetection zones. IEEE Trans Power Delivery. Jan. 2009;24(1):486–487.
[15] Bower W, Ropp M. Evaluation of islanding detection methods for utility-interactive inverters in photovoltaic systems. SANDIA REPORT, SAND2002-3591. Unlimited Release Printed November 2002.
[16] Liu F, Kang Y, Zhang Y, et al. Improved SMS anti islanding method for grid-connected converters. IET Renew Power Gener. Jan. 2010;4(1):36–42.
[17] Jeong JB, Kim HJ, Ahn KS, et al. A novel method for anti-islanding using reactive power. INTELEC 05 – Twenty-Seventh International Telecommunications Conference; 2005. p. 101–106.
[18] Wang X, Freitas W, Dinavahi V, et al. Investigation of positive feedback anti-islanding control for multiple inverter-based distributed generators. IEEE Trans Power Syst. May 2009;24(2):785–795.
[19] Menon V, Nehrir MH. A hybrid anti-islanding technique using voltage unbalance and frequency set point. IEEE Trans Power Syst. Feb. 2007;22(1):442–448.
[20] Mahat P, Chen Z, Bak-Jensen B. A hybrid islanding detection technique using average rate of voltage change and real power shift. IEEE Trans Power Delivery. April 2009;24(2):764–771.
[21] Manikonda S, Gaonkar D. Islanding detection method based on image classification technique using histogram of oriented gradient features. IET Gener Transm Distrib. 2020;14(14):2790–2799.
[22] Matic-Cuka B, Kezunovic M. Islanding detection for inverter-based distributed generation using support vector machine method. IEEE Trans Smart Grid. 2014;5(6):2676–2686.
[23] Reddy J, Pandian A, Reddy C. An efficient learning based RFMFA technique for islanding detection scheme in distributed generation systems. Appl Soft Comput. 2020;96:106638.
[24] Bhatt N, Kumar A. A passive islanding detection algorithm based on modal current and adaptive boosting. Arab J Sci Eng. 2020;45(8):6791–6801.
[25] Vyas S, Kumar R, Kavasseri R. Data analytics and computational methods for anti-islanding of renewable energy based distributed generators in power grids. Renew Sustain Energy Rev. 2017;69:493–502.
[26] Jo J, Cha H. A novel anti-islanding method using positive feedback reactive power variation. J Power Electron. 2020;20(4):991–1001.
[27] Ke J, Zhengxuan Z, Zhe Y, et al. Intelligent islanding detection method for photovoltaic power system based on Adaboost algorithm. IET Gener Transm Distrib. 2020;14(18):3630–3640.
[28] Gupta N, Garg R. Algorithm for islanding detection in photovoltaic generator network connected to low-voltage grid. IET Gener Transm Distrib. 2018;12(10):2280–2287.
[29] Chicco G, Mazza A. 100 year of symmetrical components – review. Energies. 2019;12:450.
[30] Devassy S, Singh B. Design and performance analysis of three-phase solar PV integrated UPQC. IEEE Trans Ind Appl. 2018;54(1):73–81.
[31] Iravani MR, Karimi-Ghartemani M. Online estimation of steady state and instantaneous symmetrical components. IEE Proc Gener Transm Distrib. Sep. 2013;150(5):616.
[32] Pillay P, Manyage M. Definitions of voltage unbalance. IEEE Power Eng Rev. May 2001;21(5):50–51.
[33] Singh AK, Singh GK, Mitra R. Some observations on definitions of voltage unbalance. 39th American Power Symposium; 2007.
[34] Wang G, Gao F, Liu J, et al. Design consideration and performance analysis of a hybrid islanding detection method combining voltage unbalance/total harmonic distortion and bilateral reactive power variation. CPSS Trans Power Electron Appl. March 2020;5(1):86–100.
[35] Salimi S, Koochaki A. An effective method for islanding detection based on variational mode decomposition. Electrica. 2019;19(2):135–145.